An atypical NLR gene confers bacterial wilt susceptibility in Arabidopsis

Choghag Demirjian, Narjes Razavi, Gang Yu, Baptiste Mayjonade, Lu Zhang, Fabien Lonjon, Fabien Chardon, Sébastien Carrere, Jérome Gouzy, Stéphane Genin, et al.

Plant Communications
Research article

CellPress
Partner Journal

An atypical *NLR* gene confers bacterial wilt susceptibility in *Arabidopsis*

Choghag Demirjian[1,5,7], Narjes Razavi[1,7], Gang Yu[2], Baptiste Mayjonade[1], Lu Zhang[2], Fabien Lonjon[1,4], Fabien Chardon[3], Sébastien Carrere[1], Jérome Gouzy[1], Stéphane Genin[1], Alberto P. Macho[2], Fabrice Roux[1], Richard Berthomé[1,6] and Fabienne Vailleau[1,6,*]

[1]LIPME, Université de Toulouse, INRAE, CNRS, Castanet-Tolosan, France

[2]Shanghai Center for Plant Stress Biology, CAS Center for Excellence in Molecular Plant Sciences, Chinese Academy of Sciences, Shanghai, China

[3]Université Paris-Saclay, INRAE, AgroParisTech, Institut Jean-Pierre Bourgin (IJPB), 78000 Versailles, France

[4]Present address: Department of Cell & Systems Biology, University of Toronto, Toronto, ON, Canada

[5]Present address: Department of Biology, NYU, 12 Waverly Place, New York, NY 10003, USA

[6]Senior author

[7]These authors contributed equally to this article.

***Correspondence: Fabienne Vailleau (fabienne.vailleau@inrae.fr)**

https://doi.org/10.1016/j.xplc.2023.100607

ABSTRACT

Quantitative disease resistance (QDR) remains the most prevalent form of plant resistance in crop fields and wild habitats. Genome-wide association studies (GWAS) have proved to be successful in deciphering the quantitative genetic basis of complex traits such as QDR. To unravel the genetics of QDR to the devastating worldwide bacterial pathogen *Ralstonia solanacearum*, we performed a GWAS by challenging a highly polymorphic local mapping population of *Arabidopsis thaliana* with four *R. solanacearum* type III effector (T3E) mutants, identified as key pathogenicity determinants after a first screen on an *A. thaliana* core collection of 25 accessions. Although most quantitative trait loci (QTLs) were highly specific to the identity of the T3E mutant (*ripAC*, *ripAG*, *ripAQ*, and *ripU*), we finely mapped a common QTL located on a cluster of nucleotide-binding domain and leucine-rich repeat (*NLR*) genes that exhibited structural variation. We functionally validated one of these *NLR*s as a susceptibility factor in response to *R. solanacearum*, named it *Bacterial Wilt Susceptibility 1* (*BWS1*), and cloned two alleles that conferred contrasting levels of QDR. Further characterization indicated that expression of *BWS1* leads to suppression of immunity triggered by different *R. solanacearum* effectors. In addition, we showed a direct interaction between BWS1 and RipAC T3E, and BWS1 and SUPPRESSOR OF G2 ALLELE OF skp1 (SGT1b), the latter interaction being suppressed by RipAC. Together, our results highlight a putative role for BWS1 as a quantitative susceptibility factor directly targeted by the T3E RipAC, mediating negative regulation of the SGT1-dependent immune response.

Key words: *Ralstonia solanacearum*, type III effectors, *Arabidopsis thaliana*, GWAS, *R* gene, susceptibility

Demirjian C., Razavi N., Yu G., Mayjonade B., Zhang L., Lonjon F., Chardon F., Carrere S., Gouzy J., Genin S., Macho A.P., Roux F., Berthomé R., and Vailleau F. (2023). An atypical *NLR* gene confers bacterial wilt susceptibility in *Arabidopsis*. Plant Comm. **4**, 100607.

INTRODUCTION

Plant–pathogen interaction research has witnessed many advances over the last two decades, from establishment of the well-known zigzag model (Jones and Dangl, 2006) to discovery of signaling pathways downstream of receptors (Ngou et al., 2022). Most of these discoveries result from studying interactions between single genotypes of a pathogen and a host plant. Despite the effectiveness of this approach, integrating the increasing ecologically relevant number of interactions has become an unavoidable challenge. Currently, the plant–pathogen interaction view of a clear distinction between pathogen-associated molecular pattern (PAMP)-triggered immunity (PTI) and effector-triggered immunity (ETI) has

Published by the Plant Communications Shanghai Editorial Office in association with Cell Press, an imprint of Elsevier Inc., on behalf of CSPB and CEMPS, CAS.

become blurred (Thomma et al., 2011; Cook et al., 2015; Alhoraibi et al., 2019). Our growing understanding of the role of PAMPs and effectors, and of the interacting plant responses, ranging from resistance to susceptibility, has evolved greatly, especially because quantitative disease resistance (QDR; continuum of symptoms) rather than qualitative resistance (presence/absence of symptoms) appears to be the predominant mode of resistance in nature (Roux et al., 2014). Furthermore, in contrast to genes involved in qualitative resistance, *QDR* genes encode proteins with a wide range of molecular functions (Delplace et al., 2020).

Ralstonia solanacearum, the causal agent of bacterial wilt in more than 250 plant species, relies mainly on its type 3 secretion system (T3SS) and its injected type 3 effectors (T3Es) for virulence. The pan-effectome from 140 strains of the *R. solanacearum* species complex revealed more than 100 different T3Es (Sabbagh et al., 2019). The GMI1000 wild-type (WT) strain possesses a large repertoire of T3Es, with 72 *Ralstonia* injected proteins (Rips) identified (Peeters et al., 2013; Lonjon et al., 2016). To date, a comprehensive view of how the bacterium employs its T3Es to weaken plant immunity and modulate host metabolism has been limited (Landry et al., 2020). Therefore, studying T3E mutants is one strategy for identifying their roles in bacterial virulence and in bypassing plant immunity, which is based on plant extracellular pathogen recognition receptors (PRRs) or intracellular receptors, mainly from the nucleotide-binding domain and leucine-rich repeat (NLR) protein family. However, previous studies using classical pathogenicity tests based on inoculation of the Col-5 susceptible accession of *Arabidopsis thaliana* with single T3E mutants have revealed the roles of only a small number of these effectors in bacterial virulence (Guéneron et al., 2000; Cunnac et al., 2004; Solé et al., 2012). This may be partly explained by the potential functional redundancy of some T3Es (Remigi et al., 2011) and by the use of a very restricted number of host genotypes.

Genome-wide association studies (GWAS) are powerful tools for deciphering the genetic architecture of complex traits such as QDR (Bartoli and Roux, 2017; Demirjian et al., 2023). For instance, in *A. thaliana*, the atypical Resistance-related KinaSe 1 (RKS1), which confers broad-spectrum QDR to the leaf vascular bacterial pathogen *Xanthomonas campestris* pv. *campestris*, was finely mapped by GWAS performed on both worldwide and local mapping populations (Huard-Chauveau et al., 2013; Debieu et al., 2016; Frachon et al., 2017). RKS1 was then identified as a key protein in the resistosome as well as a hub of an immune signaling pathway that largely differs from those involved in PTI and ETI (Wang et al., 2019; Delplace et al., 2020). In addition, GWAS performed on worldwide and local mapping populations of *A. thaliana* in response to *R. solanacearum* GMI1000 at 27°C revealed the well-known immune receptor pair RPS4/RRS1-R involved in bacterial wilt resistance (Aoun et al., 2017), as well as two susceptibility genes involved in response to the bacterium at elevated temperature (i.e., *AtSSL4* and *SDS*; Aoun et al., 2017, 2020). Because susceptibility genes can facilitate the infection process, support compatibility with a pathogen (van Schie and Takken, 2014; Zaidi et al., 2018), or encode immune suppressors and negative regulators of plant immunity, their modulation can confer resistance (van Schie and Takken, 2014).

Interestingly, challenging a local mapping population of *A. thaliana* with an *R. solanacearum* mutant of the key regulator of type 3 secretion, HpaP, led to identification and functional validation of three additional host susceptibility genes, *RACK1B*, *RKL1*, and *PEX3* (Demirjian et al., 2022). In contrast to numerous GWAS that have mainly challenged plants with WT strains of microorganisms, this approach focuses on single T3E mutants, thereby addressing the question of the effect of a particular pathogenicity determinant in its wild background.

In this study, we aimed at functionally validating a common QTL identified in response to key pathogenic determinants of *R. solanacearum*. We first explored the genetic diversity of response to 47 T3E mutants of GMI1000 using a core collection of 25 natural accessions from two complementary *A. thaliana* mapping populations. From analysis of this large phenotypic dataset, we then characterized the genetic architecture of the response of the highly polymorphic French TOU-A local mapping population (population A from Toulon-sur- Arroux, France; Frachon et al., 2017) to four T3E mutants (*ripAC*, *ripAG*, *ripAQ*, and *ripU*). Although most QTLs were highly specific to T3E mutants, we finely mapped a common QTL located in a cluster of *NLR* genes that exhibited structural variation identified by *de novo* sequencing of a local TOU-A accession. Strikingly, functional validation revealed that this *NLR* gene acts as a susceptibility factor in response to *R. solanacearum*, with quantitative responses depending on two alleles associated with the quantitative resistance status of the accessions. We named this gene *Bacterial Wilt Susceptibility 1* (*BWS1*). Further characterization showed that expression of *BWS1* can suppress cell death associated with ETI, with significant differences according to the *BWS1* alleles tested. We also showed that BWS1 interacts directly with the T3E RipAC. Because SGT1 has been reported to be an essential regulator of ETI, involved in regulating the accumulation and activation of NLRs (Azevedo et al., 2002; Kadota et al., 2010), we tested its interaction with BWS1. Interestingly, we showed that BWS1 interacts with SGT1b and that this interaction is suppressed by RipAC. Together, our results highlight a putative role for BWS1 as a quantitative susceptibility factor directly targeted by RipAC, mediating negative regulation of an SGT1-dependent immune response to *R. solanacearum*.

RESULTS

Forty-seven T3E mutants against 25 accessions: The natural genetic diversity of *A. thaliana* response reveals the effects of *R. solanacearum* effectors

To identify the involvement of T3Es in bacterial virulence, we explored the natural genetic diversity of response to single and multiple T3E mutants using a dedicated core collection of wild *A. thaliana* accessions. We used a core collection of 25 accessions (CC25) composed of 16 accessions maximizing the diversity present among a worldwide set of 265 accessions (McKhann et al., 2004), eight accessions spread across the genomic space of the French TOU-A local mapping population (195 accessions; Frachon et al., 2017), and the reference accession Col-0 (Supplemental Figure 1 and Supplemental Table 1). Accessions from the CC25 were inoculated with 43 *R. solanacearum* single T3E mutants, four poly-mutants corresponding to members of several T3E families (RipS, six T3Es

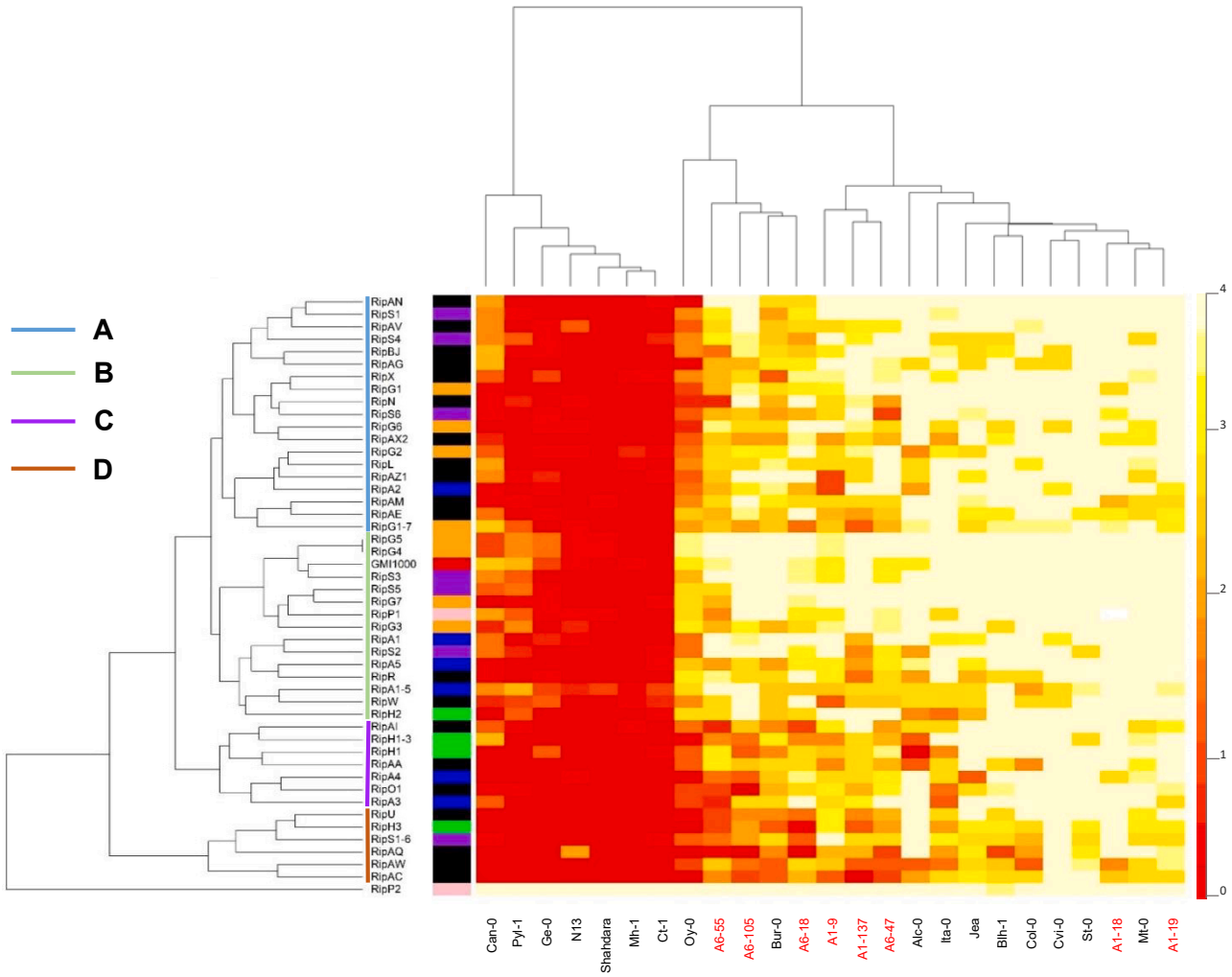

Figure 1. D-HCL presenting the natural diversity in responses of an *A. thaliana* core collection to 47 *R. solanacearum* T3E mutants at 7 days after inoculation (dai).

LSmeans were calculated at 7 dai (n = 3 plants per genotype). The colored gradient on the y axis (right) represents the scale of disease symptoms, ranging from red, which represents a disease score of 0 for a healthy plant, to yellow, which represents a disease score of 4 for a dead plant. On the x axis, the worldwide and local TOU-A accessions of *A. thaliana* are shown in black and red, respectively. The horizontal colored bars on the y axis (left) of the D-HCL represent the different *R. solanacearum* families of T3Es, with GMI1000 in red, the RipG family in orange, the RipS family in purple, the RipP family in pink, the RipA family in blue, the RipH family in green, and the single T3Es in black. The vertical colored bars on the y axis correspond to the four identified groups of T3Es. See also Supplemental Tables 1 and 2, and Supplemental Figures 1–3.

mutated; RipA, five T3Es mutated; RipG, seven T3Es mutated; and RipH, three T3Es mutated) and the GMI1000 WT strain from which the mutants were derived (Supplemental Table 2). Three plants per genotype were inoculated at 27°C with the 47 T3E mutants and GMI1000 and scored for symptoms from 3 to 7 days after inoculation (dai). A double hierarchical clustering (D-HCL) analysis was performed at each dai using the genotypic values of the 25 accessions for the disease index (Figure 1 and Supplemental Figure 2). We observed a change in the plant response to *R. solanacearum* T3E mutants along with the kinetics of disease development (Supplemental Figure 2). Disease progression resulted in the formation of two distinct groups of accessions at 7 dai. The first group was composed of seven worldwide accessions that were resistant to GMI1000 and all T3E mutants (with the exception of the *ripP2* mutant) at 7 dai (Figure 1), leading us to hypothesize that they may carry the *RRS1-R* allele (Deslandes et al., 2003) and corroborating a previous study suggesting the absence of fully resistant accessions harboring the RPS4/RRS1-R receptor pair at 27°C in the TOU-A local population (Aoun et al., 2020). The second group contained accessions from both mapping populations and showed a higher diversity of response to all 46 T3E mutants, with the exception of the *ripP2* mutant (Figure 1).

On the bacterial side, we observed four groups of T3E mutants, with GMI1000 belonging to group B (Figure 1). No overlap was observed between these four groups and TE3 families (Figure 1). A global view of the D-HCL highlighted accessions that were more resistant to 13 T3E mutants of groups C and D (*ripAI*, *ripH1-3*, *ripH1*, *ripAA*, *ripA4*, *ripO1*, *ripA3*, *ripU*, *ripH3*, *ripS1-6*, *ripAQ*, *ripAW*, and *ripAC*), including six out of the eight TOU-A accessions (Figure 1). The distinction between groups A

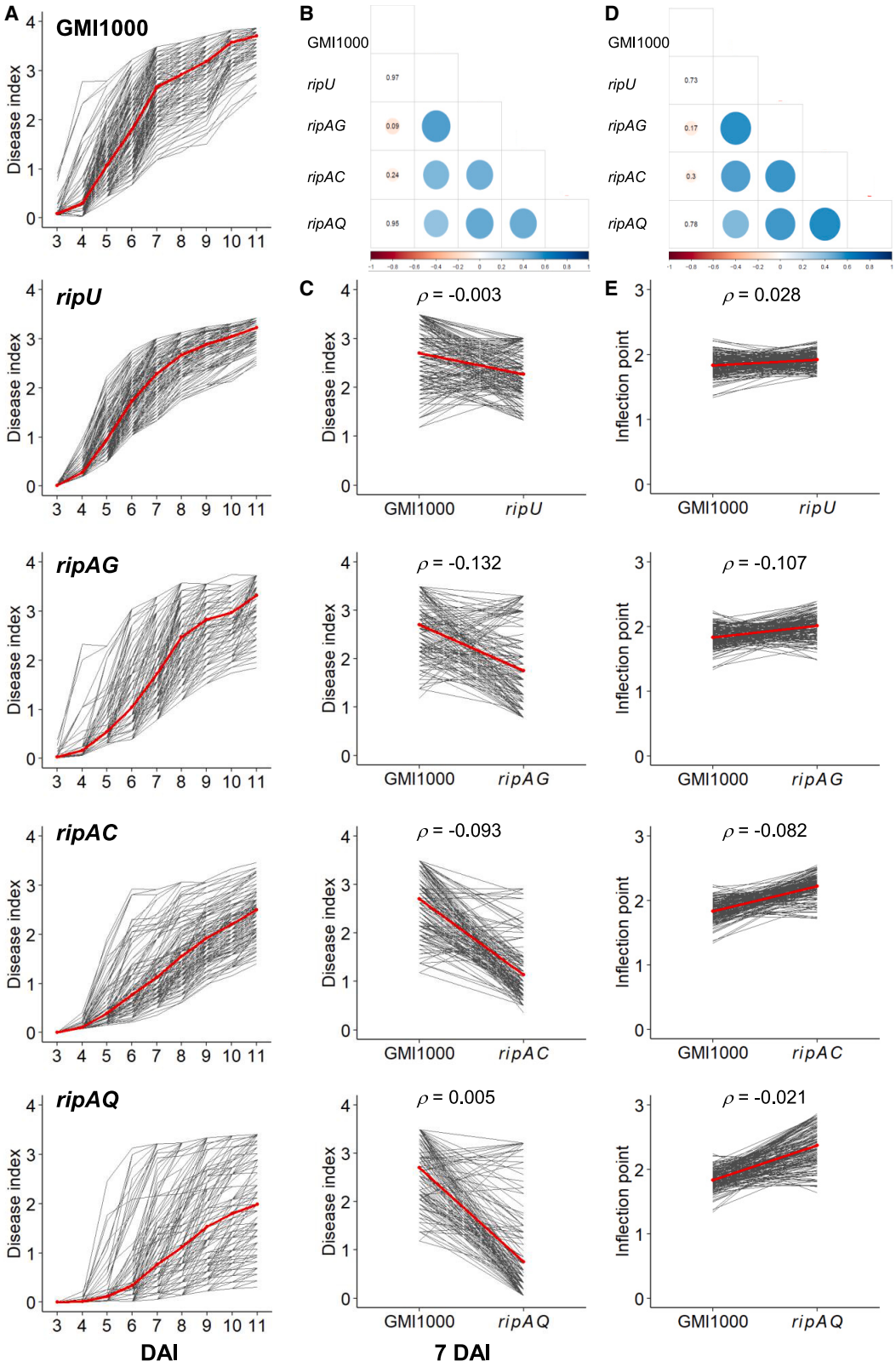

(legend on next page)

and B appears to be related to variable kinetics of response and to resistance level of accessions to T3E mutants. Moreover, a careful examination of the disease index curves highlighted a subgroup of eight T3Es in group A to which accessions showed more contrasting responses compared with GMI1000 (*ripBJ*, *ripAG*, *ripX*, *ripG1*, *ripN*, *ripS6*, *ripG6*, and *ripAX2*) (Figure 1 and Supplemental Figure 2). Based on these results, we decided to select a short list of four T3E mutants for the rest of our experiments: *ripU*, *ripAG*, *ripAC*, and *ripAQ*. We selected these mutants for (1) being hypoaggressive compared with GMI1000; (2) showing a differential kinetics of disease progression (i.e., a delay in disease establishment) (Supplemental Figure 3); (3) having peculiar protein domain composition, such as RipAC with a plant LRR domain (Guéneron et al., 2000) and RipAQ with a cyclic nucleotide-binding domain; and (4) being highly conserved in the *R. solanacearum* species complex while showing extensive sequence diversity, such as for RipAC and RipU, suggesting an extreme diversity and different evolutionary pressures (Peeters et al., 2013).

The TOU-A local mapping population reveals contrasting responses to *R. solanacearum* T3E mutants

Given the phenotypic results obtained with the CC25 and the fact that the TOU-A local population lacks the major RRS1-R resistance allele, we used the TOU-A mapping population to study the extent of natural genetic variation in response to the selected *R. solanacearum* T3E mutants. We inoculated 195 whole-genome-sequenced TOU-A accessions with the *ripU*, *ripAG*, *ripAC*, and *ripAQ* T3E mutants. We scored disease development from 3 to 11 dai (Figure 2A) and compared it with that produced by the GMI1000 WT strain (Demirjian et al., 2022; Figure 2A). With GMI1000, most accessions were susceptible at 11 dai (Figure 2A) with broad-sense heritability value estimates (H^2) above 0.3 from 3 to 11 dai (Supplemental Table 3). Interestingly, for each single T3E mutant, disease establishment was delayed in the TOU-A population and the accessions were on average, at 11 dai, less susceptible than when inoculated with GMI1000 (Figure 2A). Importantly, strong genetic variation in the response to each single T3E mutant was observed among the TOU-A accessions, with the presence of crossing reaction norms leading to a shift in the rank of the accessions between GMI1000 and each single T3E mutant (Figure 2C and Supplemental Figure 4). Consistently, the genetic correlation between GMI1000 and each T3E mutant was weak (Figure 2B). On the other hand, pairwise genetic correlations between the four T3E mutants were significantly positive (Figure 2B). Together, these results suggest both a contrasting genetic architecture between GMI1000 and each T3E mutant and common genetic response mechanisms to the four T3E mutants.

Common and specific genetic bases of response to *R. solanacearum* T3E mutants

The genome of the 195 TOU-A accessions was sequenced with Illumina technology, and reads were mapped to the Col-0 genome reference (Frachon et al., 2017), leading to identification of 1 902 592 single nucleotide polymorphisms (SNPs). To finely map the genomic regions associated with natural variation in response to GMI1000 and to the four selected T3E mutants (*ripU*, *ripAG*, *ripAC*, and *ripAQ*) at each dai, we used a mixed model taking into account the effects of population structure (Kang et al., 2010), adopting a genome-wide association approach combined with a local score (GW-LS) analysis (Bonhomme et al., 2019). For GMI1000 and each T3E mutant, we identified a polygenic architecture in which most QTLs were specific to a given inoculated strain (Supplemental Figure 5; Supplemental Tables 4–8). Comparison of the lists of QTLs identified in each of the five treatments highlighted only two QTLs on chromosomes 3 and 5 that were common to the four T3E mutants. The QTL on chromosome 3 corresponds to the *At3g43425* gene, which encodes a transposable element. On the other hand, the QTL on chromosome 5 encompasses five *NLR* genes from a genomic region composed of seven *NLR* genes (*At5g45200*, *At5g45210*, *At5g45220*, *At5g45230*, *At5g45240*, *RPS4*, and *RRS1*). This QTL, not identified in response to GMI1000, corresponds to the highest association peak at 5 dai for *ripU*, *ripAC*, and *ripAQ* and at 4 dai for *ripAG* (Supplemental Figure 5; Supplemental Tables 4–8).

In order to summarize the kinetics of disease progression, we applied for each "accession × treatment" combination a logistic S-curve model on the genotypic values obtained at each dai. We then calculated four proxies corresponding to continuous variables representative of the main stages of the complete kinetics of disease progression: (1) 10% of disease onset, (2), 50% of disease symptoms (corresponding to the inflection point), (3) 90% of disease symptoms, and (4) slope of the curve (Supplemental Table 3). We then used these four proxies to run GW-LS analyses. We observed that the proxies, with the exception of slope, were highly heritable, with the inflection point showing the highest heritability values (H^2 of 0.63, 0.40, 0.66, 0.35, and 0.78 for GMI1000, *ripU*, *ripAG*, *ripAC*, and *ripAQ* mutants, respectively; Supplemental Table 3). On average, the inflection point, which corresponded to 50% symptom development, was reached

Figure 2. Genetic diversity in plant response of the TOU-A local population to *R. solanacearum* inoculation with the GMI1000 WT strain and *ripU*, *ripAG*, *ripAC*, and *ripAQ* T3E mutants.

(A) For each time point, the best linear unbiased predictors (BLUPs) were estimated using the disease index score values. The red lines represent the mean of disease index over all accessions in response to each of the T3E mutant inoculations. Inoculations were performed on 4-week-old plants using a root inoculation method.

(B) A correlation graph of a Spearman correlation test using the BLUPs at 7 dai ($P < 0.01$, when significant no value is shown).

(C) Reaction norm curves of the WT GMI1000 vs. each T3E mutant using the BLUPs at 7 dai. The red lines represent the mean of disease index over all accessions.

(D) A correlation graph of a Spearman correlation test using the inflection point.

(E) Reaction norm curves of the WT GMI1000 vs. each T3E mutant using the inflection point. The red lines represent the mean of disease index over all accessions. The value on each graph represents the Spearman correlation rho value **(C and E)**. See also Supplemental Table 3 and Supplemental Figures 3, 4, and 12.

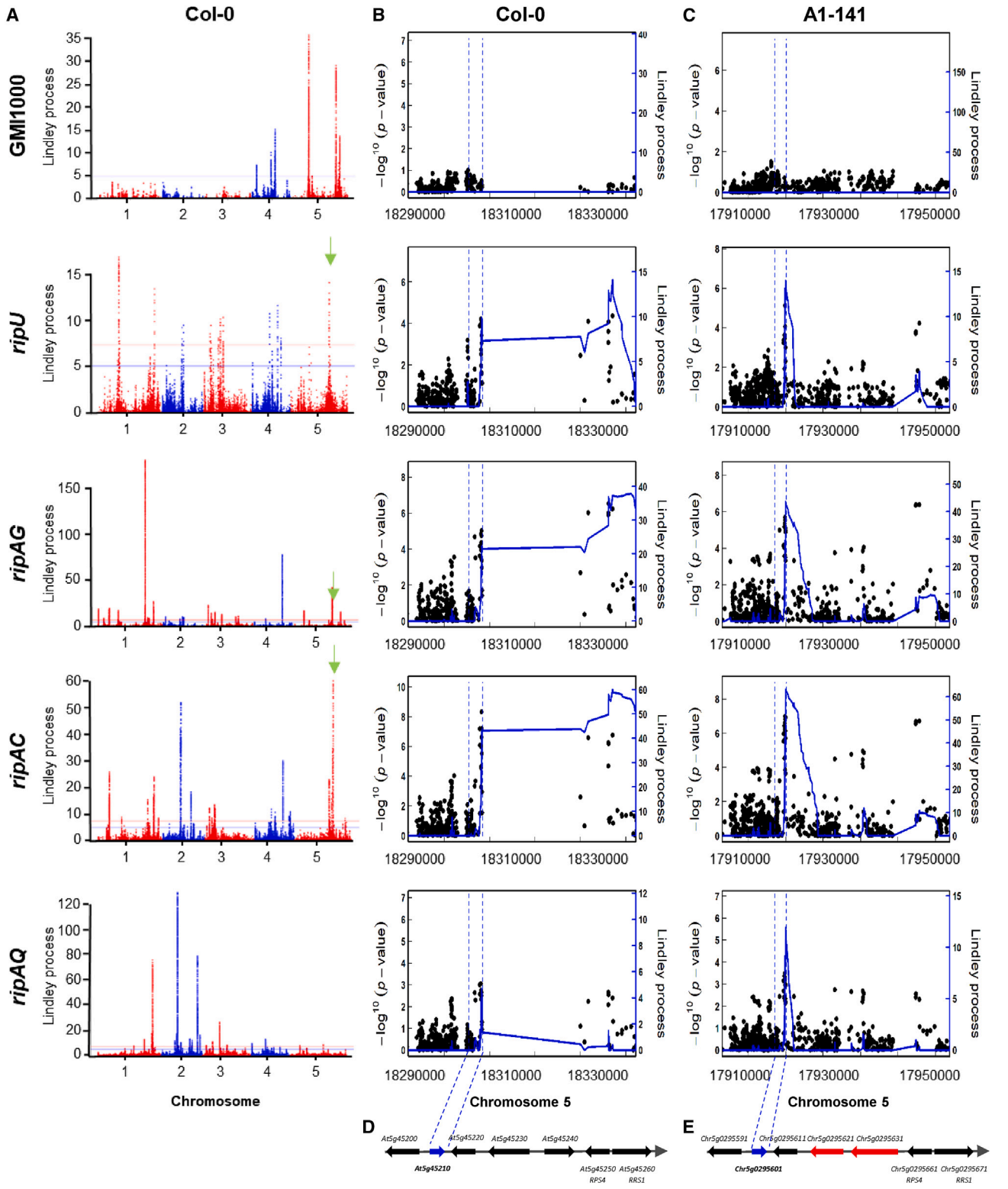

Figure 3. The genetics of QDR to *R. solanacearum* using two reference genomes.

(A) The genetics of QDR to *R. solanacearum* WT GMI1000 strain and *ripU*, *ripAG*, *ripAC*, and *ripAQ* mutants in the TOU-A population identified by GW-LS using the inflection point and mapped to the Col-0 reference genome. The green arrow represents the common QTL.

(B) Close-up view of the genomic region corresponding to the common QTL on chromosome 5 of the Col-0 reference genome (18 283 966–18 330 310 bp).

(legend continued on next page)

later in the kinetics with the mutants compared with GMI1000 (Figure 2E), consistent with the delayed disease establishment observed across accessions for each T3E mutant (Figure 2A). Similar to observations at 7 dai (Figure 2B), genetic correlations for the inflection points were significantly positive among the four T3E mutants (Figure 2D). GW-LS analyses also revealed that the QTL overlapping with the cluster of seven *NLR* genes was associated with the inflection point in response to *ripU*, *ripAC*, and *ripAG* but not *ripAQ* (Figure 3A; Supplemental Tables 9–13).

A close inspection of this common QTL (18 283 966–18, 330 310 bp) revealed the absence of SNPs over a ~20-kb genomic region located in the middle of the QTL (Figure 3B). This specificity may result from a highly conserved genomic region and a structural variation in the TOU-A population that impedes mapping of Illumina reads to the Col-0 reference genome at that location. Therefore, in order to disentangle these two hypotheses and evaluate the relevance of reanalyzing phenotype–genotype associations using a more appropriate reference genome, we sequenced the genome of the reference TOU-A1-141 accession with a long-read sequencing technology (GenBank: JAMBAT000000000). Rerunning GW-LS analyses from the SNP set called by mapping Illumina reads from the 195 accessions to the TOU-A1-141 *de novo* genome sequence resulted in similar genetic architectures, with most QTLs being specific to a given treatment (Figure 4A, Supplemental Figure 6; Supplemental Tables 14–18). We also detected the same QTL located on chromosome 5 and common to the four T3E mutants (Figure 4A). A detailed view of this genomic region revealed the presence of SNPs across the entire genomic region (17 905 260–17 961 631 bp). This discrepancy with the absence of SNPs when using the Col-0 genome as a reference resulted from the presence of a structural variation: two Col-0 *NLR* genes at this locus (*At5g45230* and *At5g45240*) were replaced by two other *NLR* genes in the A1-141 accession (At71029_*Chr5g0295621* and At71029_*Chr5g0295631*, called *Chr5g0295621* and *Chr5g0295631* hereafter; Figure 3D and 3E). In addition, the TOU-A1-141 *de novo* genome sequence allows for a better resolution in mapping candidate genes, with the identification of the association peak located on the gene *Chr5g0295601*, corresponding to *At5g45210* in Col-0 (Figure 3B–3E). This gene in Col-0 is annotated as encoding an uncharacterized putative disease-resistance protein from the Toll/interleukin-1 receptor (TIR) type-NLR class of R proteins and classified as an RRS1-like NLR (Van de Weyer et al., 2019).

An *NLR* gene conferring disease susceptibility to bacterial wilt harbors specific alleles correlated with differential responses to T3E mutants

In order to study the role of this *NLR* gene in response to *R. solanacearum*, we identified and validated three homozygous Col-0 T-DNA insertion mutants that we challenged with GMI1000 (Figure 5A, Supplemental Figure 7; Supplemental Table 19). All three mutants (*bws1.1*, *bws1.2*, and *bws1.3*) showed a delay in disease appearance, with significantly fewer wilting symptoms compared with the WT (Figure 5A; Supplemental Tables 20 and 21). These results demonstrate that the *At5g45210* gene is involved in disease susceptibility in response to *R. solanacearum* in the Col-0 background. We therefore named *At5g45210 BWS1*.

Based on nucleotide diversity of *BWS1*, the TOU-A accessions were divided into five major haplogroups, which we named alleles A to E (Supplemental Figure 8). The most common haplogroup A contains 93 accessions, and the less frequent haplogroup E contains eight accessions (Supplemental Figure 8). We then looked for putative relationships between these five haplogroups and the inflection point obtained after inoculation with GMI1000 and the four T3E mutants (Figure 4B). For the GMI1000 WT strain, no significant differences were detected among the five haplogroups (Figure 4B). By contrast, for the four T3E mutants, accessions of haplogroup E were more susceptible on average, with significantly lower values for the inflection point. On the other hand, accessions of haplogroups A, C, and D appeared to be more resistant, with accessions of haplogroup A showing the highest inflection point. The response of haplogroup B accessions appears to be highly dependent on identity of the T3E mutant (Figure 4B). To confirm the differential response to inoculation with the four T3E mutants between the haplogroups identified in the TOU-A population, we complemented the *bws1.2* mutant (named *bsw1* hereafter) with alleles of the most phylogenetically distant haplogroups (i.e., alleles of the TOU-A accessions A1-78 and A6-88 representative of the haplogroups A and E, respectively; Figure 5A; Supplemental Table 22; and Supplemental Information 1 and 2). The *BWS1* allele of accession A6-88 (haplogroup E) is very similar to the *BWS1* allele of Col-0, with fewer differences between these two alleles compared with accession A1-78 (haplogroup A) (Supplemental Table 22).

We then obtained several transgenic lines and selected two T4 homozygous lines with the highest levels of transgene expression for each construct. Transgenic lines were named *bws1*::*A1-78-1* and *bws1*::*A1-78-2* for complementation of *bws1* with the A1-78 allele and *bws1*::*A6-88-1* and *bws1*::*A6-88-2* for complementation of *bws1* with the A6-88 allele (Supplemental Figure 7C). We then challenged the four complemented lines, the *bws1* mutant, and Col-0 with the GMI1000 WT strain and the four T3E mutants. Disease index was scored from 3 to 11 dai (Figure 5B–5F; Supplemental Table 23). With GMI1000, all complemented lines showed disease symptoms at 4 dai, with disease kinetics significantly faster compared with *bws1* mutant. Interestingly, we observed a significant allelic effect: lines complemented with an

(C) Close-up view of the genomic region corresponding to the common QTL on chromosome 5 of the A1-141 reference genome (17 905 260–17 961 631 bp). The x axis indicates the physical positions of the single nucleotide polymorphisms (SNPs). The dots correspond to the −log10 *P* values of the SNPs obtained with a mixed model implemented in EMMAX software (y axis on the left). The solid blue colored curve indicates the Lindley process (local score method with $\xi = 2$) calculated from left to right (y axis on the right). The blue dashed vertical lines indicate the candidate gene (*At5g45210* or *Chr5g0295601*) intervals detected, without taking into account the right part of the curve.

(D and E) Schematic representations of the genomic region around the common QTL in the Col-0 and A1-141 genomes, respectively. The blue arrows represent the candidate genes *At5g45210* in Col-0 **(D)** and *Chr5g0295601* in A1-141 **(E)**. Red arrows represent two different genes present in A1-141 and in the TOU-A population (*Chr5g0295621* and *Chr5g0295631*), replacing the Col-0 genes at this locus (*At5g45230* and *At5g45240*). See also Supplemental Tables 4–18 and Supplemental Figures 5 and 6.

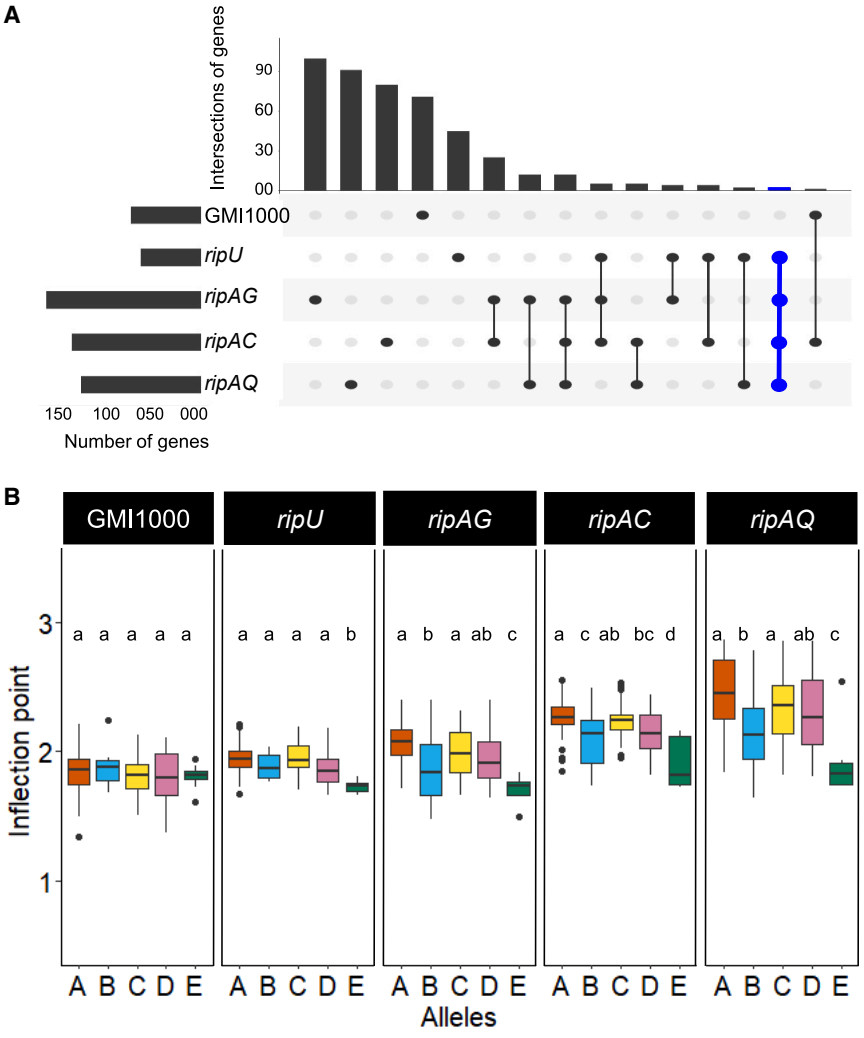

Figure 4. Identification of a common QTL in response to inoculation with T3E mutants and highlight of specific alleles on this QTL.

(A) Histogram showing the total number of genes underlying the QTLs identified by GW-LS for WT GMI1000 and the four T3E mutants using the inflection points (x axis) and the number of intersecting QTLs between the different sets of genes (y axis). In blue are highlighted the two genes *Chr5g0295601* and *Chr5g0295611*, which underlie the common QTL on chromosome 5 identified by GW-LS.

(B) Effects of the five alleles (x axis) identified in the TOU-A population for the gene *Chr5g0295601* using the inflection points (y axis). Allele A for the A1-78 accession is colored in orange, and allele E for the A6-88 accession is colored in green. Tukey's test was performed, and treatments with the same letters are not statistically different ($P < 0.05$). See also Supplemental Tables 14–18 and Supplemental Figures 6 and 7.

allele of haplogroup E were more susceptible than lines complemented with an allele of haplogroup A (Figure 5B; Supplemental Table 24). These complementation data are thus consistent with the fact that the more susceptible *BSW1* allele of accession A6-88 is phylogenetically very close to the *BSW1* allele of Col-0. These data confirm the role of *BWS1* as a susceptibility gene and the importance of allelic version in the quantitative effect on disease observed in the TOU-A population. We observed the same pattern with the T3E mutants, but with some variations and quantitative complementation phenotypes, which may depend on the aggressiveness of the T3E mutants and on the impact of the mutation in the different complemented lines. Nevertheless, in all conditions tested, the *bws1*::*A6-88* lines (allele of haplogroup E) were significantly more susceptible overall compared with the *bws1*::*A1-78* lines (allele of haplogroup A) (Figure 5B–5F; Supplemental Table 24).

BWS1 suppresses effector-triggered cell death

The main described role of NLR proteins remains the induction of ETI through the recognition of effectors (Jones and Dangl, 2006). Overexpression of NLR genes in *Nicotiana benthamiana* often leads to activation of HR-associated cell death (Jin et al., 2002). Conversely, *Agrobacterium*-mediated expression of the A1-78 *BSW1* allele (haplogroup A) and A6-88 *BSW1* allele (haplogroup E) (hereafter called *35S*:*A1-78*+ and *35S*:*A6-88*+) did not lead to cell death (Figure 6A and Supplemental Figure 9A), consistent with the putative role of BWS1 in enhancing plant susceptibility. The *R. solanacearum* T3E RipI, which has been shown to induce cell death (Xian et al., 2020; Zhuo et al., 2020), was used as a positive control (Figure 6A and Supplemental Figure 9B). To determine whether the overexpression of *BWS1* interferes with the ETI-associated HR induced by other *R. solanacearum* T3Es, we first expressed both *BWS1* alleles and *35S*:*GUS* (as a negative control) in full *N. benthamiana* leaves. One day later, *Agrobacterium* inducing the expression of different *R. solanacearum* T3Es was infiltrated in specific sectors of the same leaves. RipE1 and RipAA have been shown to induce ETI-associated cell death when expressed in *N. benthamiana* (Poueymiro and Genin, 2009; Sang et al., 2020). The results showed that expression of both *BWS1* alleles inhibited RipE1-triggered cell death, with the A1-78 allele showing a stronger suppression, but they did not suppress RipAA-triggered cell death (Figures 6C and 6D and Supplemental Figure 10). Intriguingly, the A6-88 *BWS1* allele specifically suppressed RipI-triggered cell death (Figures 6C and 6D and Supplemental Figure 10).

SGT1 contributes to the stability and activation of NLR proteins, thereby contributing to the activation of ETI (Azevedo et al., 2002; Kadota et al., 2010). RipAC has recently been show to associate with SGT1 to suppress NLR-mediated SGT1-dependent immune responses, including RipE1-induced cell death (Yu et al., 2020; Nakano et al., 2021). It is noteworthy that although BWS1 seems to act as a negative regulator of immunity, it also interacts with SGT1 (Figures 7A and 7B), suggesting that SGT1 may be associated with NLRs that act in both positive and negative regulation of immunity. Moreover,

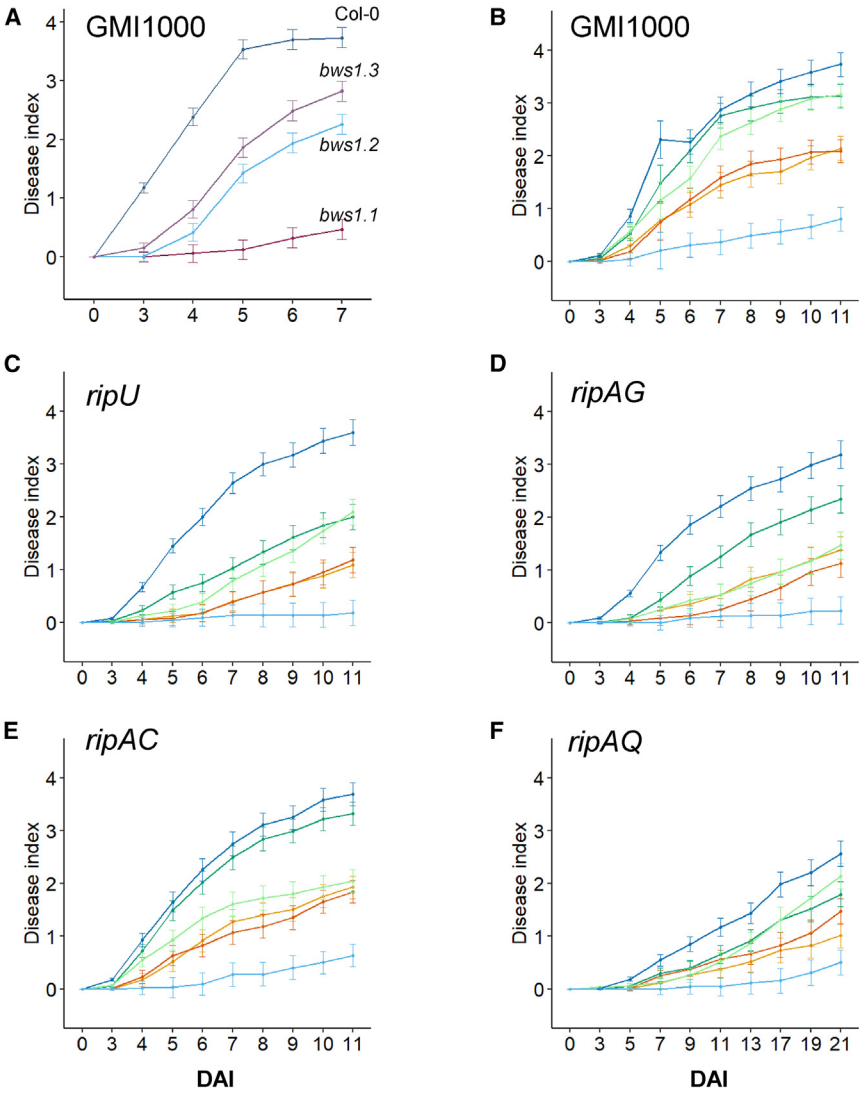

Figure 5. Comparison of wilting symptom development of the *A. thaliana bws1* mutant and its corresponding complemented lines.

(A) Dynamics of disease symptoms of *A. thaliana At5g45210* mutants in response to the GMI1000 WT strain. LSmeans ± standard errors from three independent replicates are shown (n = 48 plants per genotype). Inoculation was performed with 10^8 bacteria/ml. See Supplemental Tables 20 and 21 for statistical tests.

(B–F) Dynamics of disease symptoms of the *A. thaliana bws1* mutant (light blue) and two corresponding complemented lines with the A1-78 allele (*bws1*::*A1-78-1* in light orange and *bws1*::*A1-78-2* in dark orange) and the A6-88 allele (*bws1*::*A6-88-1* in dark green and *bws1*::*A6-88-2* in light green) compared with Col-0 (dark blue) inoculated with **(B)** GMI1000 WT, **(C)** the *ripU* mutant, **(D)** the *ripAG* mutant, **(E)** the *ripAC* mutant, and **(F)** the *ripAQ* mutant. LSmeans ± standard errors from two independent replicates are shown (n = 32 plants per genotype). Inoculation was performed with 10^7 bacteria/ml. See Supplemental Tables 23 and 24 for statistical analyses. See also Supplemental Figure 8.

we found a direct interaction between RipAC and BWS1 (Figure 7C and Supplemental Figure 11A), although, as seen after *BWS1* expression, co-expression of either *BWS1* allele in the presence of RipAC did not lead to cell death (Figure 6B and Supplemental Figure 9C). Interestingly, the interaction between BWS1 and AtSGT1b was suppressed in the presence of RipAC (Figure 7D and Supplemental Figure 11B). Together, these results reinforce a putative role of *BWS1* as a quantitative susceptibility factor and suggest targeting of the BWS1–SGT1 complex by RipAC.

DISCUSSION

A. thaliana TOU-A natural population enables the unraveling of genetic diversity related to the response to *R. solanacearum* T3E mutants

The use of a very restricted number of host plant genotypes inoculated with different T3E mutants of *R. solanacearum* and the low resulting phenotypic diversity observed have limited characterization of the role of effectors and identification of their targets (Cunnac et al., 2004). Functional redundancy was also proposed as another possible reason for this lack of phenotypic variation (Remigi et al., 2011; Solé et al., 2012). In the present study, an initial screen of an *A. thaliana* core collection with 47 T3E mutants demonstrated that functional redundancy was not, in part, responsible for the lack of phenotypic variation. Interestingly, the T3E mutants clustered differently along the kinetics of infection, suggesting a more or less important contribution of these effectors to bacterial virulence over time. These observations are consistent with the observed hierarchy in the secretion of T3Es (Lonjon et al., 2016) and during plant infection, with specific expression patterns in different plant environments (Jacob et al., 2013; de Pedro-Jové et al., 2021). Hence, their roles can be more determining in changing plant environments, according to the host genotype.

In a previous study, a worldwide collection of *A. thaliana* showed a more contrasting phenotypic response than the local TOU-A population when challenged with an *hpaP* single mutant (Demirjian et al., 2022). These contrasting phenotypes were partly explained by the recognition of RipP2/RRS1-R in many worldwide accessions, masking the identification of other putative actors in the *A. thaliana*/*R. solanacearum* molecular dialog. Here, we demonstrated that the TOU-A population is a relevant genomic resource for studying these interactions, and analysis of single T3E mutants in the *R. solanacearum* collection may have implications at two levels. First, the differences in genetic architecture observed between GMI1000 and each T3E mutant could result from direct plant responses in the absence of a given T3E. Second, the absence of one T3E could affect other molecular processes at the bacterial level, which in turn could indirectly shape the response of the TOU-A population. Moreover,

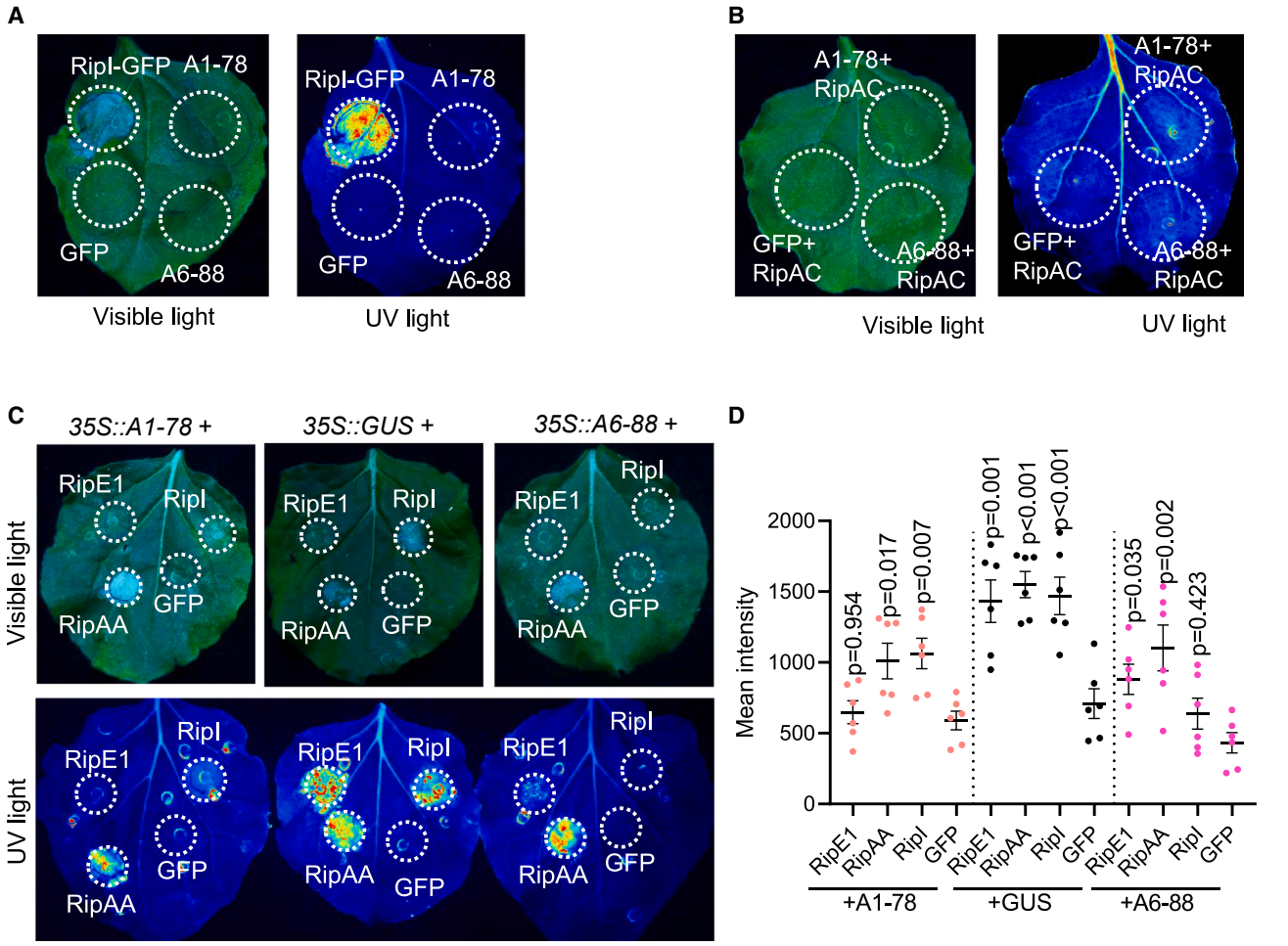

Figure 6. BWS1 does not induce cell death alone or in the presence of RipAC, and expression of *BWS1* suppresses effector-triggered cell death in *Nicotiana benthamiana*.

(A) Expression of A1-78 and A6-88 *BWS1* alleles cannot induce cell death in *N. benthamiana*. Cell death observations in *N. benthamiana* expressing different constructs. *Agrobacterium* containing different constructs (*35S*::*RipI-GFP*; *35S*::*GFP*; *35S*::*A1-78*; *35S*::*A6-88*) were infiltrated into *N. benthamiana* leaves, and the cell death phenotypes were observed 7 days post-infiltration with either visible light (upper panel, n = 6 from two independent replicates) or UV light (lower panel, n = 4 from two independent replicates). RipI-GFP was used as a positive control. RT–PCR and western blot controls are presented in Supplemental Figures 9A and 9B, respectively.

(B) Co-expression of A1-78 and A6-88 *BWS1* alleles with RipAC cannot induce cell death in *N. benthamiana*. Cell death observations in *N. benthamiana* co-expressing RipAC and different constructs. *Agrobacterium* containing different constructs (*35S*::*GFP*; *35S*::*A1-78*; *35S*::*A6-88*) and *35S*::*RipAC* (1:1 ratio) were infiltrated into *N. benthamiana* leaves, and the cell death phenotypes were observed 7 days post-infiltration with either visible light (upper panel, n = 6 from two independent replicates) or UV light (lower panel, n = 4 from two independent replicates). RT–PCR controls are presented in Supplemental Figure 9C.

(C) Cell death observations in different *N. benthamiana* plants expressing different cell death inducers. *Agrobacterium* containing different constructs (*35S*::*A1-78*; *35S*::*GUS*; *35S*::*A6-88*) were infiltrated into whole *N. benthamiana* leaves, and 1 day later *Agrobacterium* containing different cell death inducers were infiltrated in the circled areas. The cell death phenotypes were observed 7 days post-infiltration with cell death inducers using either visible light (upper panel, n = 12 from two independent replicates) or UV light (lower panel, n = 6 from two independent replicates).

(D) Cell death quantification of **(C)** in UV light conditions. Cell death is represented as intensity measured by ImageJ. Data are presented as means ± standard errors of the means, and individual data points are shown as dots. Statistical analysis was performed using ANOVA in each plant gene expression condition, and *P* values, compared with the GFP control, are labeled in the graphs. Western blot controls are presented in Supplemental Figure 10. These experiments were repeated six times with similar results. See also Supplemental Figures 9 and 10.

comparing the genotypic values obtained with the full set of accessions of the TOU-A population between GMI1000 and four selected T3E mutants brought out a remarkably different genetic architecture, which was in line with the absence of genetic correlations between GMI1000 and each of the T3E mutants. Interestingly, the reaction norm curves showed that the TOU-A accessions acted differently in each treatment with a T3E mutant, thereby reflecting different virulence mechanisms associated with each mutant, potentially related to specific plant responses.

GWAS fine-tuning: A new playground to discover

Our comparative approach and a close-up of a common QTL region called for fine-tuning of conventional GWA methods. The use

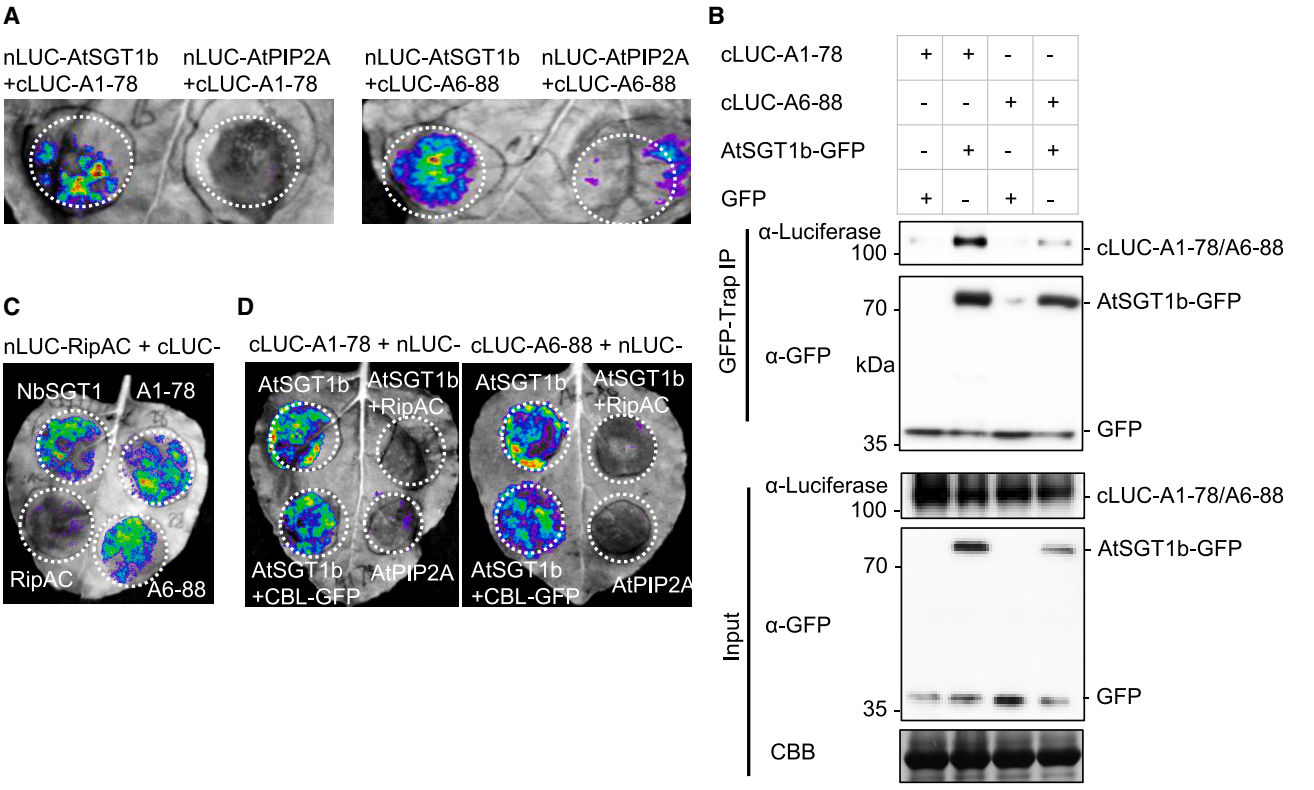

Figure 7. RipAC interrupts the interactions between BWS1 proteins and AtSGT1b.

(A) Split-LUC assays showing that both BWS1 alleles associate with AtSGT1b. The experiments were repeated twice.

(B) CoIP validates the interaction of AtSGT1b with both BWS1 alleles. Blots were stained with Coomassie brilliant blue (CBB) to verify equal loading. Three replicates were performed with similar results.

(C) Split-LUC assays showing that both BWS1 proteins associate with RipAC. CLUC-NbSGT1 was used as a positive control, and cLUC-RipAC was used as a negative control.

(D) Competitive Split-LUC assays showing that RipAC interrupts the interactions of both BWS1 proteins with AtSGT1b. Western blots showing protein accumulation are presented in Supplemental Figure 11. In **(A)** and **(D)**, nLUC-AtPIP2A + cLUC-A1-78/A6-88 combinations were used as negative controls. In all experiments, *Agrobacterium* containing different constructs were co-infiltrated into *N. benthamiana* leaf tissues as indicated, and luminescence was observed at 2 days post inoculation. Four replicates were performed with similar results. See also Supplemental Figure 11.

of an S-curve model to fit the disease index curves obtained with the different strains allowed us to get an overall picture of the infection process, including the speed of infection. The number of candidate genes identified with this S-curve model, considering the overall dynamics of kinetics, was reduced in all five GW-LS experiments compared with the daily basis analyses. Although we may consider that we are leaving aside some interesting candidates in this case, the currently highlighted genes are undeniably robust candidates for further study. Interestingly, when we compared the candidate genes identified with GMI1000 and the four mutants, no gene was found in common. Comparing the four T3E mutants alone, several specific genes were identified, and one main common candidate gene was revealed (*At5g45210*). In addition, we fine-tuned our analyses and demonstrated the importance of performing genetic mapping analyses with a sequenced reference genome that is genetically representative of the mapping population. Hence, the A1-141 reference genome brought precision to the mapping, narrowing down the QTL from five *R* genes with Col-0 to only two *R* genes with A1-141. We also confirmed that even if two *NLR* genes from this cluster (*At5g45230* and *At5g45240*) were absent in the A1-141 genome, the QTL was not associated with potential indels in the TOU-A population at this locus. We thus refined the specific QTL region and confirmed that *At5g45210* in Col-0, corresponding to *Chr5g0295601* in A1-141, was the main common candidate gene in this study. Therefore, with this work, we have improved the means of conducting association studies by using kinetics parameters and a more appropriate reference genome, thus enabling more precise identification of genes involved in plant response to a bacterial pathogen.

Shaking up the models: *BWS1* is an atypical *NLR*

The main candidate gene highlighted in this study encodes a TIR-NLR protein. NLRs are mainly described as participating in bacterial recognition, usually acting by guarding host components, which indirectly induce ETI (Pruitt et al., 2021; Yuan et al., 2021; Ngou et al., 2022). Unexpectedly, the *At5g45210* mutants showed enhanced resistance with significantly fewer wilting symptoms in response to *R. solanacearum* inoculation. We thus named *At5g45210 BWS1* because it is the first *R* gene, to our knowledge, involved in susceptibility to bacterial wilt. Remarkably, very few studies have assigned a susceptibility function to an *NLR*. For instance, *LOV1*, a *coiled-coil* (*CC*)-type

NLR, confers susceptibility to Victorian blight caused by the fungal pathogen *Cochliobolus victoriae* (Lorang et al., 2004). Interestingly, *LOV1* also mediates resistance to the biotrophic fungal pathogen *Puccinia coronata* by activating ETI (Sweat et al., 2008; Lorang et al., 2012). Another example is *LAZ5*, a *TIR-NLR* gene with similarities to the *RPS4* gene (Palma et al., 2010). *LAZ5* disruption increases QDR to *Sclerotinia sclerotiorum* (Barbacci et al., 2020). In their study, the authors suggested that *S. sclerotiorum,* a necrotrophic fungus with a broad host range, could exploit this *R* gene to its benefit.

BSW1 joins the list of susceptibility genes already identified by GWA mapping in response to *R. solanacearum* (Aoun et al., 2017, 2020; Demirjian et al., 2022). Exploiting natural genetic variation clearly enables the discovery of plant loci involved in response to pathogens, loci potentially masked in classical genetic mapping studies that explore variability in responses of a segregating population obtained after a cross between a resistant and a susceptible genotype. Here, our study reveals that *BWS1* is involved in Col-0 susceptibility to *R. solanacearum* and in QDR, with symptoms ranging from high susceptibility to resistance in the TOU-A population. Interestingly, the phenotypes obtained when transgenic complemented lines were inoculated with GMI1000 and the T3E mutants pointed out the significant quantitative effect associated with both more resistant (*A1-78*) and susceptible (*A6-88*) alleles. Therefore, we assume that the use of less armed bacteria, with selected T3Es that have potentially a broader impact on bacterial pathogenicity, enabled us to shed light on this novel and important actor in plant immunity.

In parallel to our work, recent discoveries showed that RipAC suppresses cell death triggered by RPS2, Avr3a/R3a, and several *R. solanacearum* T3Es, including RipE1, RipP1, and RipAA (Yu et al., 2020; Nakano et al., 2021). Yu et al. (2020) showed that RipAC associates with SGT1 to suppress NLR-mediated SGT1-dependent immune responses, likely by inhibiting mitogen-activated protein kinase (MAPK)-mediated phosphorylation of SGT1, which may contribute to the release and activation of NLRs. In this work, we found that RipAC has the opposite effect on BWS1, interfering with the interaction between BWS1 and SGT1b. Considering the role of BWS1 as a susceptibility factor (by negatively regulating the activation of immunity), it is tempting to speculate that RipAC may induce the release and activation of BWS1, although the exact biochemical nature of the targeting of the BWS1-SGT1b complex by RipAC will require further investigation. Overall, these data highlight the unexpected role of BWS1 as an NLR that negatively regulates ETI and suppresses *A. thaliana* immunity to *R. solanacearum* in an allele-specific manner.

BWS1, a central hub for plant immunity revealed through the study of natural diversity?

Because *BWS1* was the common candidate gene identified in response to inoculation with four T3E mutants, we may ask whether BWS1 acts alone or whether it may be a central hub, guarded by other NLRs. Indeed, *BWS1* is found within an *R* gene cluster, a common feature observed for many plant NLRs. An increasing number of examples suggest that clustered *NLR* genes are often co-expressed and may function cooperatively (Van de Weyer et al., 2019), consistent with the recent concept of a "receptor network" (Smakowska-Luzan et al., 2018; Ngou et al., 2021). For instance, it was demonstrated that NRG1, a CC-NLR, together with N, a TIR-NLR, jointly mediated resistance to tobacco mosaic virus (Peart et al., 2005). Extensive work has also demonstrated that AvrRps4 T3E from *Pseudomonas syringae* and RipP2 T3E from *R. solanacearum* are recognized by the TIR-NLR pair RRS1-R/RPS4 (Narusaka et al., 2009; Le Roux et al., 2015; Sarris et al., 2015). Accordingly, it will be interesting to look for potential BWS1 interactors on both the plant and bacterial sides.

To our knowledge, BWS1 is the first NLR identified as being involved in susceptibility to a hemibiotrophic pathogen. Therefore, studying its mode of action in plant susceptibility or quantitative resistance, depending on the plant genotype tested, will be of particular interest. However, we must bear in mind that there is a remarkable diversity in the distribution of T3Es within the different strains that make up the *R. solanacearum* species complex (Sabbagh et al., 2019). Hence, we could imagine a broader role for BWS1, and it would be particularly interesting to evaluate its putative function in response to other pathogens under more natural conditions in future experiments. This work once again shows us that the paths of immunity are complex and quantitative, and that even after 30 years of the zigzag model describing the plant immune system, we still understand only the tip of the iceberg. Integrating the genetic diversity of both partners in the model constitutes the next future challenge.

METHODS

Bacterial strains and growth media

The bacterial strains and *R. solanacearum* T3E mutants used in this study are described in Supplemental Table 2. *R. solanacearum* WT strain GMI1000 and T3E mutants were grown in complete B medium (rich medium) or minimal MP medium supplemented with 20 mM glutamate (minimal medium) (Plener et al., 2010) at 28°C. For the *ripU*, *ripAG*, *ripAC*, and *ripAQ* mutants most deeply studied in this work, we followed their growth *in vitro* to confirm that the delayed phenotypes observed on inoculated plants were not related to a potential growth deficiency. *In vitro* growth curves were measured in both minimal medium and rich medium in 96-well plates using a FLUOstar Omega microplate reader (BMG Labtech, France). Experiments were repeated twice with four technical repetitions each (Supplemental Figure 12). Strains of *Escherichia coli* and *Agrobacterium tumefaciens* were grown at 37°C and 28°C, respectively, in Luria–Bertani (LB) medium (Bertani, 1951). When needed, antibiotics were added at the following concentrations: kanamycin 25 mg l^{-1}, gentamycin 10 mg l^{-1}, ampicillin 50 mg l^{-1}, and chloramphenicol 25 mg l^{-1} for *E. coli*; kanamycin 50 mg l^{-1}, spectinomycin 40 mg l^{-1}, and gentamycin 10 mg l^{-1} for *R. solanacearum*; rifampicin 50 mg l^{-1}, kanamycin 50 mg l^{-1}, gentamycin 20 mg l^{-1}, and spectinomycin 40 mg l^{-1} for *A. tumefaciens*.

Plant material and growth conditions

The natural accessions composing the core collection CC25 used in this study are listed in Supplemental Table 1.

To investigate the natural variation in response of *A. thaliana* to the four selected *R. solanacearum* T3E mutants, 195 whole-genome-sequenced natural accessions of the French TOU-A population were used (Frachon et al., 2017; Aoun et al., 2020).

Three T-DNA insertion mutants for the *At5g45210* gene (named *bws1.1*, *bws1.2*, and *bws1.3* hereafter) were identified using the T-DNA

express *Arabidopsis* online mapping tool (http://signal.salk.edu/cgi-bin/tdnaexpress; Alonso et al., 2003) and ordered from the Nottingham Arabidopsis Stock Centre at the University of Nottingham, UK (https://arabidopsis.info/). The mutants are in the Columbia 0 genetic background (Col-0; NASC ID N70000). Col-0 and mutants were grown and genotyped as previously described (Aoun et al., 2017) using primers listed in Supplemental Table 19. PCR fragments corresponding to the flanking sequence tag were purified on 1× TAE agarose gel with the QIAquick Gel Extraction Kit (https://www.qiagen.com) and sequenced to confirm the T-DNA insertion in the *At5g45210* gene. Homozygous T3 progeny were produced. For *R. solanacearum* inoculation, GWAS, and RT–qPCR assays, accessions and transgenic lines were sown, stratified, and grown as previously described (Aoun et al., 2020).

N. benthamiana plants were grown in a walk-in chamber at 22°C under a 16-h light/8-h dark cycle and a light intensity of 100–150 mE m^{-2} s^{-1}. Four- to 5-week-old *N. benthamiana* plants were used for experiments.

Natural variation in response of a core collection of 25 *A. thaliana* accessions to 47 T3E mutants of *R. solanacearum*

Experimental design

The 25 accessions from the CC25 (Supplemental Table 1) were phenotyped in response to the GMI1000 WT strain and the 47 T3E mutants (Supplemental Table 2). For each strain, the plants were arranged in a randomized complete block design (RCBD) with three experimental blocks, each containing one replicate of each accession.

Statistical analyses

At each dai, we ran the following mixed model to explore natural genetic variation among the 25 accessions in response to GMI1000 and each of the 47 T3E mutants:

$$disease\ index_{ij} = \mu disease\ index + block_i + accession_j + \varepsilon_{ij}$$

In this model, μ is the overall phenotypic mean of disease index; "block" accounts for differences between the experimental blocks; "accession" measures the differences among the 25 accessions; and "ε" is the residual term. Inference was performed by ReML estimation using the PROC MIXED procedure in SAS v.9.4 (SAS Institute, Cary, NC, USA). The "block" term was treated as a random effect, and the "accession" term was treated as a fixed effect. Significance of the random effect was determined by likelihood ratio tests of the model with and without this effect. For the fixed effect, the term "accession" was tested over its appropriate denominator to calculate F values. At each dai, least-squares means (LSmeans) of disease index were estimated for each accession × bacterial strain combination. Because *A. thaliana* is a highly selfing species, LSmeans correspond to the genotypic values of accessions.

At each dai, a double hierarchical double clustering between the 25 accessions and the 48 bacterial strains was performed on LSmeans using the function *heatmap.2* from the *gplots* library implemented in the *R* environment.

Plant inoculation and phenotyping

In all our experiments, inoculation of intact roots was performed on 4-week-old *A. thaliana* plants, and wilting symptoms were measured as previously described (Lohou et al., 2014). In brief, plants were soaked for 20 min in 2 l per tray of a bacterial suspension with 1.10^7 or 1.10^8 bacteria/ml. Inoculated plants were then transferred to a growth chamber at 27°C (75% relative humidity, 12 h light at 100 μmol m^{-2} s^{-1}). Plants were monitored for wilting symptoms from 3 to 11 dai (21 dai for the *ripAQ* mutant) with a disease index scale ranging from 0 for healthy plants to 4 for dead plants (Morel et al., 2018).

Natural variation in response of an *A. thaliana* TOU-A mapping population to *R. solanacearum*

Experimental design

For the GWA mapping assays, 181, 190, 180, 184, and 180 accessions were phenotyped in response to the GMI1000 WT strain and *ripU*, *ripAG*, *ripAC*, and *ripAQ* mutants, respectively. For each strain, plants were arranged in an RCBD with three experimental blocks, each containing one replicate of each accession.

Statistical analyses

For each of the five treatments, a mixed model was used to explore the natural genetic variation in disease index and estimate genotypic values of accessions at each time point of phenotyping using the lme4 library in the *R* environment (RStudio Team, 2022) as described in Demirjian et al. (2022).

To describe the kinetics of disease progression for each accession × treatment combination, a logistic S curve was fitted to the genotypic values obtained for each dataset. The data were transformed as the percentage of wilted leaves, following a logistic curve with the equation:

$$genotypic\ values = 1 / (1 + exp\ (b \times (log(x) - log(e)))$$

where *b* is the steepness (slope) of the curve and *e* is the x value of the sigmoid midpoint (inflection point, at which 50% of the leaves were wilted). From the kinetic curve, we defined the onset of the curve as the day on which 10% of the leaves were wilted (disease onset 10%) and the offset of the curve as the day on which 90% of the leaves were wilted (disease offset 90%).

Spearman correlations were calculated using the best linear unbiased predictors (BLUPs) at 7 dai or the inflection point using the corrplot library in the *R* environment (RStudio Team, 2022).

GWA mapping with local score analysis

For each *R. solanacearum* strain, a mixed model implemented in EMMAX software (Efficient Mixed-Model Association eXpedited; Kang et al., 2010) was used to fine-map the genomic regions of the Col-0 and A1-141 TOU-A reference genomes associated with natural disease index variation at each phenotyping time point or with the four parameters derived from the S curve (disease onset 10%, disease offset 90%, inflection point *e*, and steepness *b*). A local score approach on the set of *P* values provided by EMMAX was then applied as described previously (Aoun et al., 2020; Demirjian et al., 2022). In brief, using a tuning parameter ξ of 2, the local score allows detection of significant genomic segments, equivalent to finding a peak, by accumulating local association signals based on *P* values, which reflect linkage disequilibrium between SNPs. Genomic segments that accumulated strong signals and underlying genes that fell in a ±2-kb window were considered.

A1-141 accession DNA extraction, genome assembly, and annotation

Genomic DNA extraction

High-molecular-weight DNA was extracted from 3-week-old plants as described in Russo et al. (2022). The purity of genomic DNA was assessed with a NanoDrop 8000 (Thermo Fisher Scientific, Waltham, MA, USA), and the integrity was determined using a Fragment Analyzer system (Agilent, CA).

Oxford Nanopore library preparation and sequencing

Ten micrograms of unsheared genomic DNA was processed using the SQK-LSK108 library preparation kit according to the manufacturer's instructions (Oxford Nanopore Technologies, Oxford, UK). The library was loaded on an R9.4.1 Flow Cell and sequenced for 72 h. Base calling was performed with Albacore version 2.1.10.

Genome assembly and gene annotation

Nanopore reads were assembled into contigs with wtdbg2 (Ruan and Li, 2020). The contigs were scaffolded using AllMaps software (Tang et al., 2015) and ordered using the Col-0 nuclear genome as a reference. The scaffolds were then polished with two rounds of Pilon (Walker et al., 2014) using Illumina paired-end reads. For each round, the paired-end reads were first mapped with bwa (Li and Durbin, 2009), and mapping results were used by Pilon software to generate the

polished consensus sequences. As the assembly contained hundreds of short contigs likely corresponding to contaminants and spurious versions of mitochondrial and chloroplast genomes, unanchored contigs were extracted from the assembly, and the following features were computed for each contig: (1) mean read depth and coverage of ONT reads (minimap2 –x map-ont), (2) mean read depth and coverage of Illumina reads (bwa –T 50; the Illumina dataset was generated independently and was not expected to contain the same contaminants), (3) GC percentage (infoseq), and (4) high-scoring taxonomic phylum computed using ncbi-blastx vs. NCBI NR database (20221210, minimum identity 50%). The table of contig features was manually curated to identify non-plant contigs and organelle fragments, and spurious contigs were removed from the assembly. Mitochondrial and chloroplast genomes were assembled independently with CANU 1.7 (Koren et al., 2017) after selection of reads mapped with minimap2 (–x map-ont) to a databank comprising the Col-0 chloroplast and mitochondrial genomes (NCBI: NC_000932 and NC_037304). Only reads spanning more than 15 kb on the mitochondrial genome and 70 kb on the chloroplast genome were retained. Two rounds of polishing were performed on the circular contigs representing organelle genomes. The sequence origin of organelle genomes was changed to match the Col-0 origin. Then, organelle genomes were fused with the nuclear genome, and a third round of Illumina-based polishing was performed on the complete genome assembly. Supplemental Table 24 provides the metrics of read data, the metrics after the main steps of the assembly, and the software, software versions, and non-default parameters used. The finalized assembly spans 119 744 458 bp. It includes 41 gaps of 100 Ns (added by AllMaps scaffolding), 29 unanchored contigs (1 740 933 bp assigned to Chr0), a mitochondrial genome of 367 345 bp, and a chloroplast genome of 153 519 bp.

Gene model prediction was performed using EuGène software version 4.2a via the integrative pipeline egnep (Sallet et al., 2019) version 1.5 (http://eugene.toulouse.inra.fr/Downloads/egnep-Linux-x86_64.1.5.tar.gz). In addition to standard tools for repeat masking and lncRNA prediction included in egnep, the Araport (Krishnakumar et al., 2015) version 11 (2016-06) of the Col-0 genome annotation was used as both a training dataset and a source of evidence. The Araport peptide database was used for similarity searches performed with NCBI-BLASTX software version 2.2.31+ (hits spanning more than 50% of the protein length were retained), and the corresponding cDNA database was used as transcriptional evidence. The cDNAs were mapped with GMAP (Wu and Watanabe, 2005) version 2017-09-05 (hits spanning more than 30% of the transcript length at a minimum identity percentage of 95 were retained).

The protocol described in Pecrix et al. (2018) was used to predict the putative functions of the proteins (including *A. thaliana* proteins tagged as "reviewed" to perform the reciprocal best-hit step).

Polymorphism detection

Raw reads from each of the 195 accessions were mapped to the Col-0 reference genome of *A. thaliana* (TAIR10) and the TOU-A reference genome A1-141 using bwa (Li and Durbin, 2009) with default settings (version 0.7.15-r1140, command: bwa mem -M). Alignments were filtered to retain only correctly matched primary hits using the SAMtools suite (Li et al., 2009; version 1.3.1, command: samtools view -f 0x02 | samtools fixmate -c -r) and to remove duplicates (command: samtools rmdup | samtools view -q 1 -F 4 -F 256). Genome-wide SNP calling was performed for each accession with SAMtools mpileup (version 1.3.1) and VarScan (Koboldt et al., 2012; version 2.4.3, command: varscan mpileup2snp –min-coverage 5 –min-reads2 4 –min-avg-qual 30 –min-var-freq 0.8 –p-value 0.01). All polymorphic positions across accessions were recalled using the VarScan mpileup2cns command to identify missing values for non-polymorphic positions. Finally, we retained only bi-allelic positions (excluding insertions and deletions) for which fewer than half of the accessions had missing data and the alternative allele was present in at least 97% of the supporting accessions (Supplemental Table 25).

BWS1 phylogenetic tree

To construct the *BWS1* phylogenetic tree, we extracted the genomic region corresponding to *Chr5g0295601* (17 917 026–17 920 116 bp) from the TOU-A accessions and aligned the TOU-A SNPs to the A1-141 genome using the MUSCLE alignment method in MEGA version X (Kumar et al., 2018). We examined the evolutionary relationships among the accessions with a phylogenetic tree using the neighbor-joining statistical model and the bootstrap method with 500 bootstrap replications.

Statistical analyses

For each transgenic line phenotyped after inoculation with *R. solanacearum*, the following

mixed model was used to test whether a specific transgenic plant differed from the WT background:

$$disease\ index\ ij = \mu + block\ i + genotype\ j + block\ i \times genotype\ j + \varepsilon\ ij$$

where μ is the overall mean of the phenotypic data, "block" accounts for differences in micro-environmental conditions among the experimental blocks, "genotype" corresponds to the genetic differences between the transgenic line and the WT background, "block × genotype" accounts for variation in genotype differences among blocks, and "ε" is the residual term. All factors were considered to be fixed. The model was applied separately to each transgenic line and corresponding background. This model was implemented with the function lm() in the R software environment (RStudio Team, 2022). The dynamics of mutant responses to *R. solanacearum* were visualized using the ggplot2 package (https://ggplot2.tidyverse.org), showing the LSmeans ± the standard error of the LSmeans.

Generation of plasmid constructs, transgenic plants, and *R. solanacearum* mutants

The primers and plasmids used for complementation of the *bws1* mutant are listed in Supplemental Table 19. In brief, alleles A (A1-78) and E (A6-88) of *BWS1* were PCR amplified using attB1_*BWS1*_AD/attB2_*BW1*_A and attB1_*BWS1*_AD/attB2_*BW1*_D primers, respectively. PCR reactions were performed in a final volume of 25 μl, and 2 μl of genomic DNA from each accession (~10 ng/μl) was added to a PCR master mix composed of 1 μl (10 pM) of each primer, 0.5 μl (10 mM) dNTPs, 0.625 U long-range PrimeSTAR GXL DNA polymerase (TAKARA BIO, http://www.takara-bio.com), 5 μl 5× PrimeSTAR GXL buffer, and 14.5 μl sterilized water. The PCR cycling conditions were as follows: 98°C for 2 min; 30 cycles of 98°C for 10 sec, 60°C for 15 sec, and 68°C for 3.5 min. The corresponding PCR fragments were purified on 1× TAE agarose gel with the QIAquick Gel Extraction Kit. PCR products were transferred by BP reaction to the pDONR207 subcloning vector using Gateway technology according to the manufacturer's instructions (Invitrogen, Carlsbad, CA, USA). Following electroporation into *E. coli* competent cells, colonies harboring the plasmid were identified by PCR using the pDONR 207_ promoter/pDONR 207_ terminator primer pair. PCR reactions were performed in a final volume of 25 μl, with 2 μl of a bacterial colony resuspended in sterile water added to a PCR master mix composed of 0.5 μl (10 pM) of each primer, 0.5 μl (10 mM) dNTPs, 0.2 μl (10 u/μl) GoTaq DNA polymerase (Promega, Madison, WI, USA), 5 μl 5× GoTaq buffer, and 16.3 μl sterilized water. The PCR cycling conditions were as follows: 95°C for 2 min; 35 cycles of 95°C for 30 sec, 52°C for 30 sec, and 72°C for 2 min. Two colonies harboring the entry plasmid for each allele were cultivated at 37°C overnight in LB liquid medium. Plasmid DNA was extracted using the Wizard Plus SV Minipreps DNA purification system (Promega, Madison, WI, USA) and verified by EcoRV/SacI restriction enzyme digestion and Sanger sequencing. Plasmids harboring the A or D allele were then transferred by an LR reaction (Gateway system) to the pAM-PAT D35S

GWY 3HA binary destination vector (Bernoux et al., 2008) and electroporated into *A. tumefaciens* strain GV301. Transformed colonies were verified by PCR using the 35S-promoter_LR PAMPAT/35S-terminator_LR PAMPAT primer pair. The *bws1.2* mutant was then agroinfiltrated by the floral dip method (Clough and Bent, 1998). Presence of the T-DNA was confirmed by PCR using specific primers (Supplemental Table 19) with the same conditions used for genotyping of mutants. Expression levels of alleles A and E were monitored in 12 independent transgenic lines, and two independent T4 homozygous complemented lines expressing the A and E alleles at the same level of the *BWS1* gene WT control (Col-0) were selected for each allele.

Fifteen T3E mutant constructs were generated: seven using the omega interposon (Prentki and Krisch, 1984), five with the pCZ367 disruption vector (Cunnac et al., 2004), and three using cre-lox-mediated unmarked deletions (Angot et al., 2006), as described previously (Supplemental Table 2). Constructs were introduced into *R. solanacearum* GMI1000 (Salanoubat et al., 2002) by natural transformation, and genetic structure of the transformants was checked by PCR.

A1-78 and A6-88 were amplified and cloned into pDONR-207 as entry clones and subsequently cloned into destination vectors by LR reaction, generating pGWB502-A1-78 and pGWB502-A6-88 with no epitope tag and pGWB-cLUC-A1-78 and pGWB-cLUC-A6-88 for the split-luciferase assay. The constructs were confirmed by sequencing and transformed into *A. tumefaciens* GV3101. Agrobacteria containing the following constructs were described previously: pGWB502-RipAC, pGWB505-RipE1-GFP, pGWB505-RipI-GFP, pGWB511-GUS-FLAG, pGWB512-FLAG-RipAA, pGWB505-GFP, pGWB-AtSGT1b-nLUC, pGWB-AtPIP2A-nLUC, and pGWB-nLUC-RipAC (Sang et al., 2020; Xian et al., 2020; Yu et al., 2020).

Cell death observations and quantification

To observe elicitor-triggered cell death, *A. tumefaciens* GV3101 carrying different constructs were used for leaf infiltration of *N. benthamiana* plants. To observe the effect of RipAC on NLR-related cell death, *A. tumefaciens* GV3101 carrying RipAC were co-infiltrated with A1-78 or A6-88 at a 1:1 ratio (optical density 600 [OD_{600}] = 0.5 for each strain). To observe the suppression activity of A1-78 and A6-88, agrobacteria containing different constructs (A1-78, A6-88, GUS-FLAG, OD_{600} = 0.5 for each strain) were infiltrated, and agrobacteria containing cell death elicitors were infiltrated 1 day later into the same leaves. Cell death phenotypes were recorded by digital camera or a BIO-RAD Gel Doc XR^+ system with Image Lab software (settings: filter, Standard Filter 1; light, UV Trans illumination) 7 days post inoculation (Yu et al., 2020). The cell death intensities were quantified using ImageJ. Leaf tissues were sampled for western blotting and RT–PCR to confirm gene expression 2 days post inoculation.

Split-luciferase complementation assay

A split-luciferase complementation (Split-LUC) assay was used to investigate protein–protein interactions as described previously (Yu et al., 2020; Wang et al., 2021). *A. tumefaciens* strains containing the indicated plasmids were infiltrated into *N. benthamiana* leaves, and images were obtained with a NightShade LB 985 system (Berthold, Bad Wildbad, Germany). Protein accumulation was determined by immunoblotting.

Co-immunoprecipitation

The co-immunoprecipitation (coIP) assay was performed as described previously (Yu et al., 2020). In brief, around 1 g of *N. benthamiana* leaf tissue was collected at 2 days after infiltration with *A. tumefaciens* and frozen in liquid nitrogen. Total proteins were extracted with protein extraction buffer (100 mM Tris–HCl [pH 8], 150 mM NaCl, 10% glycerol, 5 mM EDTA, 10 mM DTT, 2 mM PMSF, 10 mM NaF, 10 mM Na_2MoO_4, 2 mM $NaVO_3$, 1% (v/v) NP-40, and 1% (v/v) plant protease inhibitor cocktail [Yeasen, China]), and immunoprecipitation was performed with 15 μl of GFP-trap beads (Smart-Life Sciences, China). Beads were washed four times with wash buffer containing 0.5% NP-40. Proteins were stripped from the beads by boiling in 40 μl of Laemmli buffer for 10 min at 70°C. The immunoprecipitated proteins were separated on SDS–PAGE gels for western blot analysis with the indicated antibodies. Blots were stained with Coomassie brilliant blue (CBB) to verify equal loading.

RNA preparation, RT–PCR, and immunoblot analysis

RNA extractions and RT–qPCR analyses to determine the expression level of *BWS1* in T-DNA insertion mutants and transgenic complemented lines were performed as described previously (Demirjian et al., 2022) using two leaves from non-infected plants. The primer pairs used are listed in Supplemental Table 19. After validation and phenotyping of the *bws1* T-DNA insertion lines, we chose to continue the experiments with complementation of the *bws1.2* mutant because it has a single T-DNA insertion, in contrast to the *bws1.1* mutant, which has multiple T-DNA insertions.

RNA preparation, RT–PCR, and immunoblots were performed to demonstrate gene expression and protein accumulation as described previously (Yu et al., 2020). Collected tissues were ground with a Tissue Lyser (Qiagen, Hilden, Nordrhein Westfalen, Germany). Total RNA was prepared with the E.Z.N.A. Plant RNA kit (Omega Bio-Tek, Norcross, GA, USA), and 1 μg of RNA was used to prepare cDNA with the ToneScript First-Strand cDNA Synthesis Kit (Toneker Biotech, Shanghai, China) with a volume of 20 μl. A1-78 and A6-88 expression were determined by RT–PCR with primers (AT5G45210-F, TCAGAATAACTACTCGTACGACCAGGT AGC; AT5G45210-R, CCGCAGTTTGTACGGACGTCCCTTATGATA), and *NbEF1a* was used as the internal reference (*NbEF1a*-F, CACGCAT TGCTTGCTTTCA; *NbEF1a*-R, TCCATCTTGTTACAGCAGCAAATC). To determine protein accumulation, ground *N. benthamiana* samples were resuspended in protein extraction buffer (100 mM Tris [pH 8], 150 mM NaCl, 10% glycerol, 1% IGEPAL, 5 mM EDTA, 5 mM DTT, 1% protease inhibitor cocktail, 2 mM PMSF, 10 mM Na_2MoO_4, 10 mM NaF, and 2 mM Na_3VO_4). The resulting protein samples were boiled at 70°C for 10 min in Laemmli buffer and loaded onto SDS–PAGE gels for western blotting. All immunoblots were analyzed using appropriate antibodies as indicated in the figures.

DATA AVAILABILITY

The A1-141 TOU-A reference genome described in this study (Supplemental Table 25) has been deposited at DDBJ/ENA/GenBank under the accession JAMBAT000000000. The version described in this paper is version JAMBAT010000000. The genome annotation is available at https://doi.org/10.25794/reference/df_vb3r0. Raw data used for genome assembly are available at NCBI SRA under the following accessions: SRR3725284, SRR19287349, and SRR19308733.

SUPPLEMENTAL INFORMATION

Supplemental information is available at *Plant Communications Online*.

FUNDING

This work was supported by the Laboratoire d'Excellence (LABEX) TULIP (ANR-10-LABX-41). C.D. was funded by a grant from the Lebanese University, and we thank INRAE, Campus France, and the INRAE Plant Health and Environment division (SPE) for their support and funding. N.R. benefited from a PhD grant co-financed by the Occitanie Regional Council and the INRAE Plant Health and Environment division (SPE). F.L. was funded by a grant from the French Ministry of National Education and Research. A1-141 sequencing was performed in collaboration with the GeT core facility, Toulouse, France (http://get.genotoul.fr) and was supported by France Génomique National infrastructure, funded as part of the Investissement d'avenir program managed by Agence Nationale de la Recherche (contract ANR-10-INBS-09).

AUTHOR CONTRIBUTIONS

Conceptualization, F.V., R.B., A.M., and F.R.; methodology, F.V., R.B., F.R., and F.C.; formal analysis, C.D. and F.R.; investigation, N.R., C.D., G.Y., L.Z., F.L., A.M., R.B., and F.V.; resources, B.M., S.C., J.G., S.G., and F.R.; data curation, S.C., B.M., and J.G.; writing – original draft, C.D., R.B., A.M., and F.V.; writing – review & editing, all the authors; funding acquisition, F.V.; supervision, R.B., A.M., and F.V.

ACKNOWLEDGMENTS

We would like to thank Barbara Ribeiro-Gomes for help with phenotyping assays and Henri Desaint for assistance with the R script for allele analysis. We thank Anne Claire Cazalé for the pACC839 construct, Patrick Barberis for help in constructing T3E mutants, Cyril Libourel for help in the principal-component analysis on the TOU-A population, and Céline Remblière for her advice to generate the transgenic lines. No conflict of interest is declared.

Received: July 29, 2022
Revised: January 19, 2023
Accepted: April 20, 2023
Published: April 25, 2023

REFERENCES

Alhoraibi, H., Bigeard, J., Rayapuram, N., Colcombet, J., and Hirt, H. (2019). Plant immunity: the MTI-ETI model and beyond. Curr. Issues Mol. Biol. **30**:39–58.

Alonso, J.M., Stepanova, A.N., Leisse, T.J., et al. (2003). Genome-wide insertional mutagenesis of *Arabidopsis thaliana*. Science **301**:653–657.

Angot, A., Peeters, N., Lechner, E., et al. (2006). *Ralstonia solanacearum* requires F-box-like domain-containing type III effectors to promote disease on several host plants. Proc. Natl. Acad. Sci. USA **103**:14620–14625.

Aoun, N., Tauleigne, L., Lonjon, F., Deslandes, L., Vailleau, F., Roux, F., and Berthomé, R. (2017). Quantitative disease resistance under elevated temperature: genetic basis of new resistance mechanisms to *Ralstonia solanacearum*. Front. Plant Sci. **8**:1387.

Aoun, N., Desaint, H., Boyrie, L., Bonhomme, M., Deslandes, L., Berthomé, R., and Roux, F. (2020). A complex network of additive and epistatic quantitative trait loci underlies natural variation of *Arabidopsis thaliana* quantitative disease resistance to *Ralstonia solanacearum* under heat stress. Mol. Plant Pathol. **21**:1405–1420.

Azevedo, C., Sadanandom, A., Kitagawa, K., Freialdenhoven, A., Shirasu, K., and Schulze-Lefert, P. (2002). The RAR1 interactor SGT1, an essential component of *R* gene-triggered disease resistance. Science **295**:2073–2076.

Barbacci, A., Navaud, O., Mbengue, M., Barascud, M., Godiard, L., Khafif, M., Lacaze, A., and Raffaele, S. (2020). Rapid identification of an *Arabidopsis NLR* gene as a candidate conferring susceptibility to *Sclerotinia sclerotiorum* using time-resolved automated phenotyping. Plant J. **103**:903–917.

Bartoli, C., and Roux, F. (2017). Genome-wide association studies in plant pathosystems: toward an ecological genomics approach. Front. Plant Sci. **8**:763.

Bernoux, M., Timmers, T., Jauneau, A., Brière, C., de Wit, P.J.G.M., Marco, Y., and Deslandes, L. (2008). RD19, an *Arabidopsis* cysteine protease required for RRS1-R-mediated resistance, is relocalized to the nucleus by the *Ralstonia solanacearum* PopP2 effector. Plant Cell **20**:2252–2264.

Bertani, G. (1951). Studies on lysogenesis. I. The mode of phage liberation by lysogenic *Escherichia coli*. J. Bacteriol. **62**:293–300.

Bonhomme, M., Fariello, M.I., Navier, H., Hajri, A., Badis, Y., Miteul, H., Samac, D.A., Dumas, B., Baranger, A., Jacquet, C., and Pilet-Nayel, M.L. (2019). A local score approach improves GWAS resolution and detects minor QTL: application to *Medicago truncatula* quantitative disease resistance to multiple *Aphanomyces euteiches* isolates. Heredity **123**:517–531.

Clough, S.J., and Bent, A.F. (1998). Floral dip: a simplified method for Agrobacterium-mediated transformation of *Arabidopsis thaliana*. Plant J. **16**:735–743.

Cook, D.E., Mesarich, C.H., and Thomma, B.P.H.J. (2015). Understanding plant immunity as a surveillance system to detect invasion. Annu. Rev. Phytopathol. **53**:541–563.

Cunnac, S., Occhialini, A., Barberis, P., Boucher, C., and Genin, S. (2004). Inventory and functional analysis of the large Hrp regulon in *Ralstonia solanacearum*: identification of novel effector proteins translocated to plant host cells through the type III secretion system. Mol. Microbiol. **53**:115–128.

de Pedro-Jové, R., Puigvert, M., Sebastià, P., Macho, A.P., Monteiro, J.S., Coll, N.S., Setúbal, J.C., and Valls, M. (2021). Dynamic expression of *Ralstonia solanacearum* virulence factors and metabolism-controlling genes during plant infection. BMC Genom. **22**:170.

Debieu, M., Huard-Chauveau, C., Genissel, A., Roux, F., and Roby, D. (2016). Quantitative disease resistance to the bacterial pathogen *Xanthomonas campestris* involves an *Arabidopsis* immune receptor pair and a gene of unknown function. Mol. Plant Pathol. **17**:510–520.

Delplace, F., Huard-Chauveau, C., Dubiella, U., Khafif, M., Alvarez, E., Langin, G., Roux, F., Peyraud, R., and Roby, D. (2020). Robustness of plant quantitative disease resistance is provided by a decentralized immune network. Proc. Natl. Acad. Sci. USA **117**:18099–18109.

Demirjian, C., Razavi, N., Desaint, H., Lonjon, F., Genin, S., Roux, F., Berthomé, R., and Vailleau, F. (2022). Study of natural diversity in response to a key pathogenicity regulator of *Ralstonia solanacearum* reveals new susceptibility genes in *Arabidopsis thaliana*. Mol. Plant Pathol. **23**:321–338.

Demirjian, C., Vailleau, F., Berthomé, R., and Roux, F. (2023). Genome-wide association studies in plant pathosystems: success or failure? *Trends Plant Sci* **Dec 13**:S1360–S1385.

Deslandes, L., Olivier, J., Peeters, N., Feng, D.X., Khounlotham, M., Boucher, C., Somssich, I., Genin, S., and Marco, Y. (2003). Physical interaction between RRS1-R, a protein conferring resistance to bacterial wilt, and PopP2, a type III effector targeted to the plant nucleus. Proc. Natl. Acad. Sci. USA **100**:8024–8029.

Frachon, L., Libourel, C., Villoutreix, R., Carrère, S., Glorieux, C., Huard-Chauveau, C., Navascués, M., Gay, L., Vitalis, R., Baron, E., et al. (2017). Intermediate degrees of synergistic pleiotropy drive adaptive evolution in ecological time. Nat. Ecol. Evol. **1**:1551–1561.

Guéneron, M., Timmers, A.C., Boucher, C., and Arlat, M. (2000). Two novel proteins, PopB, which has functional nuclear localization signals, and PopC, which has a large leucine-rich repeat domain, are secreted through the hrp-secretion apparatus of *Ralstonia solanacearum*. Mol. Microbiol. **36**:261–277.

Huard-Chauveau, C., Perchepied, L., Debieu, M., Rivas, S., Kroj, T., Kars, I., Bergelson, J., Roux, F., and Roby, D. (2013). An atypical kinase under balancing selection confers broad-spectrum disease resistance in *Arabidopsis*. PLoS Genet. **9**, e1003766.

Jacob, F., Vernaldi, S., and Maekawa, T. (2013). Evolution and conservation of plant NLR functions. Front. Immunol. **4**:297.

Jin, H., Axtell, M.J., Dahlbeck, D., Ekwenna, O., Zhang, S., Staskawicz, B., and Baker, B. (2002). NPK1, an MEKK1-like mitogen-activated protein kinase kinase kinase, regulates innate immunity and development in plants. Dev. Cell **3**:291–297.

Jones, J.D.G., and Dangl, J.L. (2006). The plant immune system. Nature **444**:323–329.

Kadota, Y., Shirasu, K., and Guerois, R. (2010). NLR sensors meet at the SGT1-HSP90 crossroad. Trends Biochem. Sci. **35**:199–207.

Kang, H.M., Sul, J.H., Service, S.K., Zaitlen, N.A., Kong, S.-Y., Freimer, N.B., Sabatti, C., and Eskin, E. (2010). Variance component model to account for sample structure in genome-wide association studies. Nat. Genet. **42**:348–354.

Koboldt, D.C., Zhang, Q., Larson, D.E., Shen, D., McLellan, M.D., Lin, L., Miller, C.A., Mardis, E.R., Ding, L., and Wilson, R.K. (2012). VarScan 2: somatic mutation and copy number alteration discovery in cancer by exome sequencing. Genome Res. **22**:568–576.

Koren, S., Walenz, B.P., Berlin, K., Miller, J.R., Bergman, N.H., and Phillippy, A.M. (2017). Canu: scalable and accurate long-read assembly via adaptive k-mer weighting and repeat separation. Genome Res. **27**:722–736.

Krishnakumar, V., Hanlon, M.R., Contrino, S., Ferlanti, E.S., Karamycheva, S., Kim, M., Rosen, B.D., Cheng, C.-Y., Moreira, W., Mock, S.A., et al. (2015). Araport: the *Arabidopsis* information portal. Nucleic Acids Res. **43**:D1003–D1009.

Kumar, S., Stecher, G., Li, M., Knyaz, C., and Tamura, K. (2018). Mega X: molecular evolutionary genetics analysis across computing platforms. Mol. Biol. Evol. **35**:1547–1549.

Landry, D., González-Fuente, M., Deslandes, L., and Peeters, N. (2020). The large, diverse, and robust arsenal of *Ralstonia solanacearum* type III effectors and their in planta functions. Mol. Plant Pathol. **21**:1377–1388.

Le Roux, C., Huet, G., Jauneau, A., Camborde, L., Trémousaygue, D., Kraut, A., Zhou, B., Levaillant, M., Adachi, H., Yoshioka, H., et al. (2015). A receptor pair with an integrated decoy converts pathogen disabling of transcription factors to immunity. Cell **161**:1074–1088.

Li, H., and Durbin, R. (2009). Fast and accurate short read alignment with Burrows-Wheeler transform. Bioinformatics **25**:1754–1760.

Li, H., Handsaker, B., Wysoker, A., Fennell, T., Ruan, J., Homer, N., Marth, G., Abecasis, G., and Durbin, R.; 1000 Genome Project Data Processing Subgroup (2009). The sequence alignment/map format and SAMtools. Bioinformatics **25**:2078–2079.

Lohou, D., Turner, M., Lonjon, F., et al. (2014). HpaP modulates type III effector secretion in *Ralstonia solanacearum* and harbours a substrate specificity switch domain essential for virulence. Mol. Plant Pathol. **15**:601–614.

Lonjon, F., Turner, M., Henry, C., Rengel, D., Lohou, D., van de Kerkhove, Q., Cazalé, A.C., Peeters, N., Genin, S., and Vailleau, F. (2016). Comparative secretome analysis of *Ralstonia solanacearum* type 3 secretion-associated mutants reveals a fine control of effector delivery, essential for bacterial pathogenicity. Mol. Cell. Proteomics **15**:598–613.

Lorang, J.M., Carkaci-Salli, N., and Wolpert, T.J. (2004). Identification and characterization of victorin sensitivity in Arabidopsis thaliana. Mol. Plant Microbe Interact. **17**:577–582.

Lorang, J., Kidarsa, T., Bradford, C.S., Gilbert, B., Curtis, M., Tzeng, S.-C., Maier, C.S., and Wolpert, T.J. (2012). Tricking the guard: exploiting plant defense for disease susceptibility. Science **338**:659–662.

McKhann, H.I., Camilleri, C., Bérard, A., Bataillon, T., David, J.L., Reboud, X., Le Corre, V., Caloustian, C., Gut, I.G., and Brunel, D. (2004). Nested core collections maximizing genetic diversity in *Arabidopsis thaliana*. Plant J. **38**:193–202.

Morel, A., Peeters, N., Vailleau, F., Barberis, P., Jiang, G., Berthomé, R., and Guidot, A. (2018). Plant pathogenicity phenotyping of *Ralstonia solanacearum* strains. Methods Mol. Biol. **1734**:223–239.

Nakano, M., Ichinose, Y., and Mukaihara, T. (2021). *Ralstonia solanacearum* type III effector RipAC targets SGT1 to suppress effector-triggered immunity. Plant Cell Physiol. **61**:2067–2076.

Narusaka, M., Shirasu, K., Noutoshi, Y., Kubo, Y., Shiraishi, T., Iwabuchi, M., and Narusaka, Y. (2009). RRS1 and RPS4 provide a dual Resistance-gene system against fungal and bacterial pathogens. Plant J. **60**:218–226.

Ngou, B.P.M., Ahn, H.-K., Ding, P., and Jones, J.D.G. (2021). Mutual potentiation of plant immunity by cell-surface and intracellular receptors. Nature **592**:110–115.

Ngou, B.P.M., Ding, P., and Jones, J.D.G. (2022). Thirty years of resistance: zig-zag through the plant immune system. Plant Cell **34**:1447–1478. https://doi.org/10.1093/plcell/koac041.

Palma, K., Thorgrimsen, S., Malinovsky, F.G., Fiil, B.K., Nielsen, H.B., Brodersen, P., Hofius, D., Petersen, M., and Mundy, J. (2010). Autoimmunity in *Arabidopsis acd11* is mediated by epigenetic regulation of an immune receptor. PLoS Pathog. **6**, e1001137.

Peart, J.R., Mestre, P., Lu, R., et al. (2005). NRG1, a CC-NB-LRR protein, together with N, a TIR-NB-LRR protein, mediates resistance against tobacco mosaic virus. Curr. Biol. **15**:968–973.

Pecrix, Y., Staton, S.E., Sallet, E., Lelandais-Brière, C., Moreau, S., Carrère, S., Blein, T., Jardinaud, M.-F., Latrasse, D., Zouine, M., et al. (2018). Whole-genome landscape of Medicago truncatula symbiotic genes. Nat. Plants **4**:1017–1025.

Peeters, N., Carrère, S., Anisimova, M., Plener, L., Cazalé, A.C., and Genin, S. (2013). Repertoire, unified nomenclature and evolution of the Type III effector gene set in the *Ralstonia solanacearum* species complex. BMC Genom. **14**:859.

Plener, L., Manfredi, P., Valls, M., and Genin, S. (2010). PrhG, a transcriptional regulator responding to growth conditions, is involved in the control of the type III secretion system regulon in *Ralstonia solanacearum*. J. Bacteriol. **192**:1011–1019.

Poueymiro, M., and Genin, S. (2009). Secreted proteins from *Ralstonia solanacearum*: a hundred tricks to kill a plant. Curr. Opin. Microbiol. **12**:44–52.

Prentki, P., and Krisch, H.M. (1984). In vitro insertional mutagenesis with a selectable DNA fragment. Gene **29**:303–313.

Pruitt, R.N., Locci, F., Wanke, F., Zhang, L., Saile, S.C., Joe, A., Karelina, D., Hua, C., Fröhlich, K., Wan, W.-L., et al. (2021). The EDS1-PAD4-ADR1 node mediates *Arabidopsis* pattern-triggered immunity. Nature **598**:495–499.

Remigi, P., Anisimova, M., Guidot, A., Genin, S., and Peeters, N. (2011). Functional diversification of the GALA type III effector family contributes to *Ralstonia solanacearum* adaptation on different plant hosts. New Phytol. **192**:976–987.

Roux, F., Voisin, D., Badet, T., Balagué, C., Barlet, X., Huard-Chauveau, C., Roby, D., and Raffaele, S. (2014). Resistance to phytopathogens e tutti quanti: placing plant quantitative disease resistance on the map. Mol. Plant Pathol. **15**:427–432.

RStudio Team. (2022). RStudio: Integrated Development Environment for R (RStudio, PBC).

Ruan, J., and Li, H. (2020). Fast and accurate long-read assembly with wtdbg2. Nat. Methods **17**:155–158.

Russo, A., Mayjonade, B., Frei, D., Potente, G., Kellenberger, R.T., Frachon, L., Copetti, D., Studer, B., Frey, J.E., Grossniklaus, U., and Schlüter, P.M. (2022). Low-input high-molecular-weight DNA extraction for long-read sequencing from plants of diverse families. Front. Plant Sci. **13**, 883897.

Sabbagh, C.R.R., Carrere, S., Lonjon, F., Vailleau, F., Macho, A.P., Genin, S., and Peeters, N. (2019). Pangenomic type III effector database of the plant pathogenic *Ralstonia spp*. PeerJ **7**, e7346.

Salanoubat, M., Genin, S., Artiguenave, F., Gouzy, J., Mangenot, S., Arlat, M., Billault, A., Brottier, P., Camus, J.C., Cattolico, L., et al. (2002). Genome sequence of the plant pathogen *Ralstonia solanacearum*. Nature **415**:497–502.

Sallet, E., Gouzy, J., and Schiex, T. (2019). EuGene: an automated integrative gene finder for eukaryotes and prokaryotes. Methods Mol. Biol. **1962**:97–120.

Sang, Y., Yu, W., Zhuang, H., Wei, Y., Derevnina, L., Yu, G., Luo, J., and Macho, A.P. (2020). Intra-strain elicitation and suppression of plant immunity by *Ralstonia solanacearum* type-III effectors in *Nicotiana benthamiana*. Plant Commun. **1**, 100025.

Sarris, P.F., Duxbury, Z., Huh, S.U., Ma, Y., Segonzac, C., Sklenar, J., Derbyshire, P., Cevik, V., Rallapalli, G., Saucet, S.B., et al. (2015). A plant immune receptor detects pathogen effectors that target WRKY transcription factors. Cell **161**:1089–1100.

Smakowska-Luzan, E., Mott, G.A., Parys, K., Stegmann, M., Howton, T.C., Layeghifard, M., Neuhold, J., Lehner, A., Kong, J., Grünwald, K., et al. (2018). An extracellular network of *Arabidopsis* leucine-rich repeat receptor kinases. Nature **553**:342–346.

Solé, M., Popa, C., Mith, O., Sohn, K.H., Jones, J.D.G., Deslandes, L., and Valls, M. (2012). The *awr* gene family encodes a novel class of *Ralstonia solanacearum* type III effectors displaying virulence and avirulence activities. Mol. Plant Microbe Interact. **25**:941–953.

Sweat, T.A., Lorang, J.M., Bakker, E.G., and Wolpert, T.J. (2008). Characterization of natural and induced variation in the *LOV1* gene, a CC-NB-LRR gene conferring victorin sensitivity and disease susceptibility in *Arabidopsis*. Mol. Plant Microbe Interact. **21**:7–19.

Tang, H., Zhang, X., Miao, C., Zhang, J., Ming, R., Schnable, J.C., Schnable, P.S., Lyons, E., and Lu, J. (2015). ALLMAPS: robust scaffold ordering based on multiple maps. Genome Biol. **16**:3.

Thomma, B.P.H.J., Nürnberger, T., and Joosten, M.H.A.J. (2011). Of PAMPs and effectors: the blurred PTI-ETI dichotomy. Plant Cell **23**:4–15.

Van de Weyer, A.-L., Monteiro, F., Furzer, O.J., Nishimura, M.T., Cevik, V., Witek, K., Jones, J.D.G., Dangl, J.L., Weigel, D., and Bemm, F. (2019). A species-wide inventory of *NLR* genes and alleles in *Arabidopsis thaliana*. Cell **178**:1260–1272.e14.

van Schie, C.C.N., and Takken, F.L.W. (2014). Susceptibility genes 101: how to be a good host. Annu. Rev. Phytopathol. **52**:551–581.

Walker, B.J., Abeel, T., Shea, T., Priest, M., Abouelliel, A., Sakthikumar, S., Cuomo, C.A., Zeng, Q., Wortman, J., Young, S.K., and Earl, A.M. (2014). Pilon: an integrated tool for comprehensive microbial variant detection and genome assembly improvement. PLoS One **9**, e112963.

Wang, J., Hu, M., Wang, J., Qi, J., Han, Z., Wang, G., Qi, Y., Wang, H.-W., Zhou, J.-M., and Chai, J. (2019). Reconstitution and structure of a plant NLR resistosome conferring immunity. Science **364**, eaav5870.

Wang, Y., Zhao, A., Morcillo, R.J.L., et al. (2021). A bacterial effector protein uncovers a plant metabolic pathway involved in tolerance to bacterial wilt disease. Mol. Plant. **14**:1281–1296.

Wu, T.D., and Watanabe, C.K. (2005). GMAP: a genomic mapping and alignment program for mRNA and EST sequences. Bioinformatics **21**:1859–1875.

Xian, L., Yu, G., Wei, Y., Rufian, J.S., Li, Y., Zhuang, H., Xue, H., Morcillo, R.J.L., and Macho, A.P. (2020). A bacterial effector protein hijacks plant metabolism to support pathogen nutrition. Cell Host Microbe **28**:548–557.e7.

Yu, G., Xian, L., Xue, H., Yu, W., Rufian, J.S., Sang, Y., Morcillo, R.J.L., Wang, Y., and Macho, A.P. (2020). A bacterial effector protein prevents MAPK-mediated phosphorylation of SGT1 to suppress plant immunity. PLoS Pathog. **16**, e1008933.

Yuan, M., Jiang, Z., Bi, G., Nomura, K., Liu, M., Wang, Y., Cai, B., Zhou, J.-M., He, S.Y., and Xin, X.-F. (2021). Pattern-recognition receptors are required for NLR-mediated plant immunity. Nature **592**:105–109.

Zaidi, S.S.-E.-A., Mukhtar, M.S., and Mansoor, S. (2018). Genome editing: targeting susceptibility genes for plant disease resistance. Trends Biotechnol. **36**:898–906.

Zhuo, T., Wang, X., Chen, Z., Cui, H., Zeng, Y., Chen, Y., Fan, X., Hu, X., and Zou, H. (2020). The *Ralstonia solanacearum* effector RipI induces a defence reaction by interacting with the bHLH93 transcription factor in *Nicotiana benthamiana*. Mol. Plant Pathol. **21**:999–1004.